

RE: A point-to-point response to reviewers' comments

“Oxygenated products formed from OH-initiated reactions of trimethylbenzene: Autoxidation and accretion” (acp-2020-165) by Yuwei Wang, Archit Mehra, Jordan E. Krechmer, Gan Yang, Xiaoyu Hu, Yiqun Lu, Andrew Lambe, Manjula Canagaratna, Jianmin Chen, Douglas Worsnop, Hugh Coe, Lin Wang

Dear Prof. Dr. Markus Ammann,

We are very grateful to the helpful comments from the reviewers, and have carefully revised our manuscript accordingly. A point-to-point response to the comments, which are repeated in *italic*, is given below.

We are looking forward to the reviewers' feedback and your decision with the revision.

Best regards,

Lin Wang
Fudan University
lin_wang@fudan.edu.cn

Reviewer #1

GENERAL COMMENTS

In this manuscript the authors present results of an experimental study of the products of the reaction of trimethylbenzene isomers with OH radicals in the absence and presence of NO_x. Reactions are conducted in a flow tube reactor and gas-phase products are analyzed using three types of online mass spectrometry that in combination allow detection of products ranging from very low to very high oxidation state. The authors detect a variety of monomer and dimer products that are not currently incorporated into the Master Chemical Mechanism, which is widely used to model the atmospheric chemistry of organic compounds. The authors propose structures for the compounds (they are preliminary since only elemental formulas and deuterium labeling data are available) and mechanisms by which they could be formed. Fortunately, the authors have kept the paper concise, and not attempted to overinterpret the results or overwhelm readers with data. Although it is difficult to judge the importance of the results because of the lack of quantitative analysis, aromatics are an important class of compounds whose chemistry is not well understood, the work is technically sound, and it should be useful for others to build on. I think the paper should be published in ACP after the following minor comments and have been addressed.

Response. We are very grateful to the positive viewing of our manuscript by Reviewer #1, and have now revised our manuscript accordingly.

SPECIFIC COMMENTS

1. Line 227-228: *How can an oxidation product have an oxidation state lower than TMB?*

Response. In the original manuscript, these products refer to ions of C₈H₁₅O⁺, C₈H₁₅O₂⁺, C₈H₁₇O⁺, and C₈H₁₇O₂⁺ detected only by Vocus PTR, all of which have very low signal intensities ranging from 14.67 cps to 78.47 cps. As a comparison, the ion counts for the most abundant C₉ products (C₉H₁₁O⁺) and C₈ products (C₈H₁₁O⁺) detected by Vocus PTR were 13887 cps and 5023 cps, respectively. The concentrations of these ions should be quite low, considering the high sensitivity of Vocus PTR to compounds with a few oxygen atoms (around 8000 cps/ppb to xylene and TMB, and 8500 cps/ppb to methyl ethyl ketone as calibrated with a commercial calibration cylinder). At the same time, there is a documented history of fragmentation during PTR ionization, leading to a leakage of oxygen atom(s) (de Gouw and Warneke, 2007; Gueneron et al., 2015; Karl et al., 2018; Tani, 2013; Yuan et al., 2017). Though oxygenated VOCs are reported to be less significantly fragmented than alkanes and many alkenes (Yuan et al., 2017), a leakage of oxygen due to fragmentation is typically on the order of < 5% for ketones, 15% for aldehydes, < 5% for ethers, <10% for carboxylic acids, 30% for peroxides, 40% for diols, and 70% for alcohols (Karl et al., 2018; Španěl and Smith, 2013). Hence, we postulate that these ions might come from fragmentation of parent compounds in the FIMR (focusing ion-molecule reactor) of Vocus PTR. We have removed this statement in Line 225-228 of the original manuscript and updated Figure 2.

The revised Figure 2 is shown below.

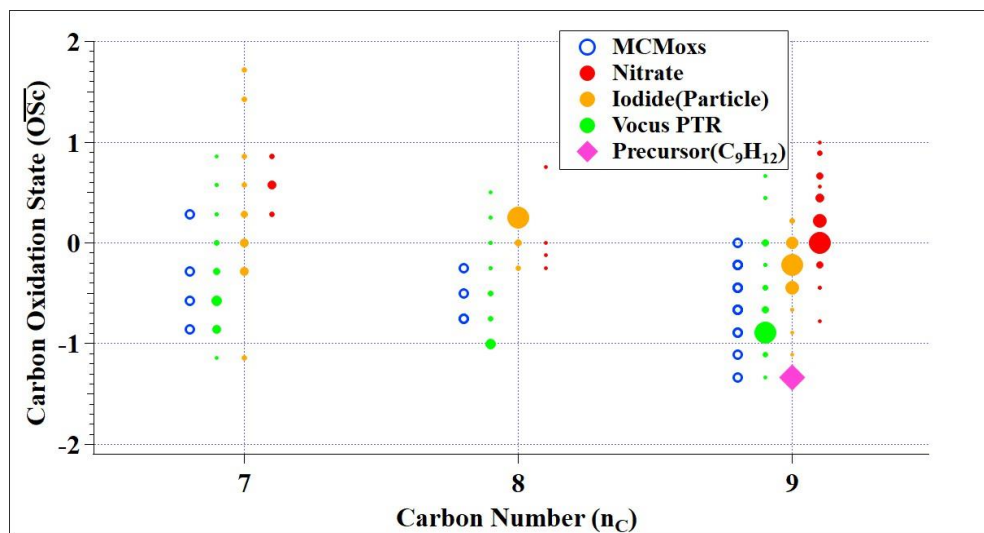


Figure 2

2. Lines 260-262 (and elsewhere): Because of the high sensitivity of the nitrate-CIMS to oxidized products I do not think you can assume that products formed in these experiments did not involve multiple OH reactions. For example, in the work by Krechmer et al., *EST* (2016) they formed multigeneration products in chamber experiments in which the lights were only on for 10 s.

Response. We agree with this reviewer that multiple OH attacks can occur in our reaction system, which is evidenced by the observation of C₉H₁₆O₆₋₉ products, as 16 hydrogen atoms in the molecular formula can be regarded as a characteristic of the second-generation products according to Molteni et al. (2018). In fact, we mentioned the possibility of multiple OH-attacks in multiple places in our manuscript, i.e., statements in Line 238 of the original manuscript and Table 2.

In Line 260-262 of the original manuscript, we intended to state that C₉H₁₂O₆ as a multi-generation hydroperoxyl product as predicted by MCM should not have a comparable yield as that formed through the carbonyl termination reaction of a peroxy radical that is involved in autoxidation, since a multi-generation product is not favored at OH exposure as short as one life time of TMB. C₉H₁₄O₆ is another product predicted by MCM but we missed it in main text of the original manuscript. C₉H₁₄O₆ is unlikely to be formed with a considerable yield through the MCM route for a similar reason.

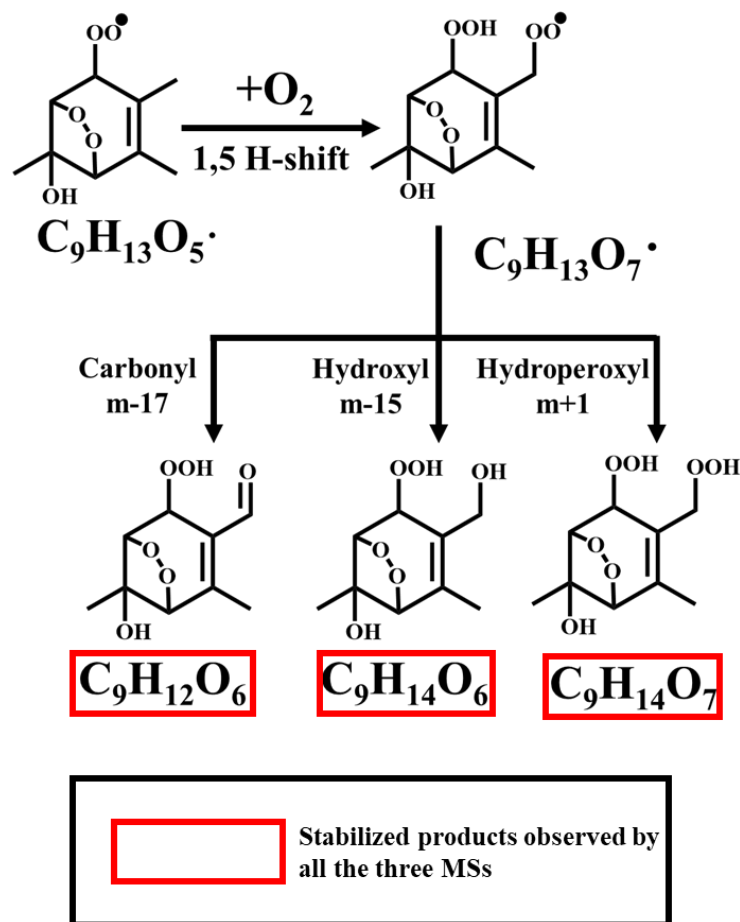
To avoid misunderstanding, we have revised our manuscript, which (Line 268-275) reads “C₉H₁₂O₆ is one of the only two signals that have been predicted by MCM,..., which is unlikely to contribute a lot to the observed signal of C₉H₁₂O₆ since the concentration of a multi-generation product is not expected to be high at OH exposure as short as one lifetime of TMB. C₉H₁₄O₆ is the other one, presumed to be a hydroperoxyl product of a second-generation peroxy radical formed via the epoxy-oxy pathway (MCM name: TM124MUOOH), which is unlikely to be formed through the MCM route with a considerable yield, either.”

Please also refer to our response to Comment #3 from Reviewer #2.

3. Line 325-326: The proposed isomerization of the bicyclic alkoxy radical would never compete with ring-opening pathways. See Vereecken and Peeters, PCCP (2009, 2010) estimation methods for these pathways.

Response. Thanks for pointing out this issue. After a detailed discussion with Dr. Vereecken, quote, “For this structure, consider that the H-migration is across a trans-substituted alkene: the $\text{CH}_3\text{-C}=\text{C-CHO}\cdot$ carbons are all in one plane. Furthermore, because of the ring structure, the $\text{CHO}\cdot$ group cannot rotate the oxygen towards the CH_3 H-atom. Hence, to shift, the H-atom would have to “leap” almost 5 angstroms without being attached to anything, whereas normally it is less than 1.4 angstroms from either or both of the starting-C/ending-O atom”, we agree with reviewer and Dr. Vereecken that the 1, 5-H-shift of this alkoxy radical is virtually impossible, and have deleted this pathway in the revised manuscript.

We have updated Scheme 1 as shown below, where the formation of $\text{C}_9\text{H}_{12}\text{O}_6$, $\text{C}_9\text{H}_{14}\text{O}_6$, and $\text{C}_9\text{H}_{14}\text{O}_7$ was proposed with the involvement of an autoxidation step.



Scheme 1

The text in Line 324-327 of the original manuscript have been deleted. We now state in the revised manuscript that (Line355-358)“An autoxidation reaction pathway that can explain the observation of $C_9H_{10}D_2O_7$ in the 1,2,4-(1-methyl-D3)-TMB + OH experiment is currently unavailable, although we speculate that a “peroxy-alkoxy-peroxy” conversion is likely involved during the formation of $C_9H_{12}O_7$ according to the number of oxygen atoms” .

4. Line 362: Please provide support (such as references) for the assumption of identical charging efficiencies. Given the high sensitivity of the nitrate-CIMS to oxidation state and chemical structure this sounds like a very poor assumption. I suspect this makes the fractions quoted in sections 3.3 and 3.4 misleading and possibly results in wrong conclusions. The only way I think one can deal with this is to always refer to these as a comparison of fractional signals or some such thing.

Response. We believe that this assumption is the best option when there are no real measurements. Hyttinen et al. (2015) modelled the charging of highly oxygenated products from cyclohexene ozonolysis using nitrate-CIMS, showing a similar charging efficiency of nitrate source for highly oxygenated compounds. Ehn et al. (2014) assumed that the nitrate source has the same sensitivity for all highly oxygenated molecules. We agree with this reviewer that nitrate-CIMS is quite sensitive to the oxidation state of compounds to be measured. However, once a compound is highly oxygenated (i.e., contains 6 or more oxygen atoms) or has at least two hydrogen bond donor functional groups (for example, hydroperoxide, OOH), it can be assumed to be charged at the collision limit (Ehn et al, 2014; Hyttinen et al., 2015). Clearly, HOM monomer and dimer contain more than two hydrogen bond donor functional groups or 6 or more oxygen atoms. Though dimers possess more functional groups that favor the binding with NO_3^- than monomers do, the charging efficiency cannot be higher than collision limit.

We have cited the above references to support our assumption, which (Line 379-380) reads “The charging efficiency for C9 and C18 products is assumed to be identical in Nitrate CI-APi-TOF (Ehn et al., 2014; Hyttinen et al., 2015)”.

5. Line 407-409: Can you distinguish peroxy nitrates by time profiles, since they should decay by reversible decomposition on short timescales (though they may be reformed)?

Response. This is a good point. However, during our experimental procedure, we focused more on the establishment of stable signals of key products, which was determined by multiple factors including wall loss, and did not try to tackle the stability of products by terminating the reaction and monitoring the decay of signals. Thus, a comparison of time profiles of various nitrogen-containing products is currently not available.

TECHNICAL COMMENTS

1. Line 289: Should be “summarizes”.

Response. We have replaced “summaries” with “summarizes”.

2. Line 345: Should be “more O atoms”.

Response. We have revised our manuscript accordingly.

3. Line 362: Should replace “charge” with “charging” or “ionization”.

Response. We have replaced “charge” with “charging”.

4. Line 457: Delete “a”.

Response. We have removed this “a”.

5. Line 459: Should be “linearly dependent”.

Response. We have revised the text as “linearly dependent on”.

Reviewer #2

The authors describing experimental results of the OH radical initiated oxidation of different trimethylbenzenes carried out in a flow-through apparatus at atmospheric pressure in air. OH has been produced via 254 nm photolysis of ozone in presence of water vapour. Qualitative results of end product analysis are provided from three mass spec techniques. The authors chose relatively high initial reactant concentrations, $(3.5 - 5.2) \times 10^{12}$ molecules cm^{-3} , with a reactant conversion of 62.3 % each within the overall residence time of 80 s. Nothing is said regarding the RO₂ radical profiles in the experiments. It can be assumed from the stated reaction parameters that RO₂ levels are substantially higher than atmospheric. Consequently, especially RO₂ self- and cross reactions are favoured, which are of less importance for the RO₂ fate under atmospheric conditions. Thus, it's not so surprising that a very big fraction of C18 products has been detected. And that's my main concern: Are the observed product distributions from these experiments relevant for the atmosphere?

Response. Indeed, the initial reactant concentrations are much higher than those under atmospheric conditions. However, high concentrations of VOCs were deliberately chosen in this study. We aim to experimentally observe highly oxygenated products to confirm the possibility of autoxidation, and to propose the detailed autoxidation pathways via the comparison between reactions of un-deuterated and partially deuterated reactants. High concentrations of reactants will certainly help identify the highly oxygenated products that are of low volatility and easy to loss. At the same time, we did not over-interpret our results by hinting that the observed product distributions from the experiments are the same as those in the ambient atmosphere. Our viewpoints in section 3.3, where the characteristics of C18 products are discussed, are (1) to confirm the extensive existence of highly oxygenated RO₂ radicals, in other words, the extensive existence of the autoxidation pathways in the OH-initiated oxidation of TMB as an echo of the last sentence in section 3.1; (2) to provide an evidence on the structural enhancement in accretion product formation. In summary, what we have focused on is the formation mechanism and chemical fates of the RO₂ radicals and HOM products.

To clarify this point, we now state in our revised manuscript (Line 217-220) that “Also note that the concentrations of precursors in our experiments were much higher than the atmospheric ones. These concentrations were deliberately chosen to help identify the highly oxygenated products that are of low volatility and easy to loss in the sampling, but subject to the side effect that the relative significance of different pathways could be altered”

and Line (423-425) that “Again, it should be noted that this result was obtained under the condition of very high concentrations of precursors and thus the relative fractions of products could be different under ambient conditions”.

Some other points that should be considered:

1. - Line 137 – 141: Why did the authors take nitrous oxide as precursor for NO and NO₂?

Response. Parts-per-million (ppm) levels of O₃ are required to generate OH radicals, which prevent sustained NO_x (especially NO) mixing ratios at sufficient levels to compete with HO₂ as a sink for RO₂, due to the fast conversion of NO_x to nitric acid (HNO₃) via the reactions of NO+O₃→NO₂+O₂ and NO₂+OH→HNO₃. On the other hand, N₂O is a better NO_x precursor specifically in OFR studies for the following reasons, as described in Lambe et al. (2017) and Peng et al. (2018), and recently reviewed in Peng et al. (2020):

- 1) The spatial distribution of NO and NO₂ generated via the N₂O + O(¹D) reaction is more homogenous than what is achieved by simple additions of NO and/or NO₂, because of the continuous production of O(¹D) from the O₃ photolysis inside the reactor.
- 2) Steady-state mixing ratios of NO from O(¹D) + N₂O reactions are orders of magnitude higher than that from a simple NO injection

2. And again here: What is the NO and NO₂ profile in the experiments? One example from modelling should be given in the manuscript in order to allow the readership to get an impression for this.

Response. Thanks for this suggestion. We utilized a photochemical model (PAM_chem_v8) (Lambe et al., 2017; Li et al., 2015; Peng et al., 2015) to investigate the NO_x concentrations and NO/NO₂ profiles in the OFR. Unfortunately, the NO/NO₂ concentrations in the model output (tens of ppb) are much larger than our reported values (a few ppb) in our Table 2 of the original manuscript, whereas the comparison of [O₃] and [1,2,4-TMB] between modelled values and measured ones looks fine (Figures R1 and R2).

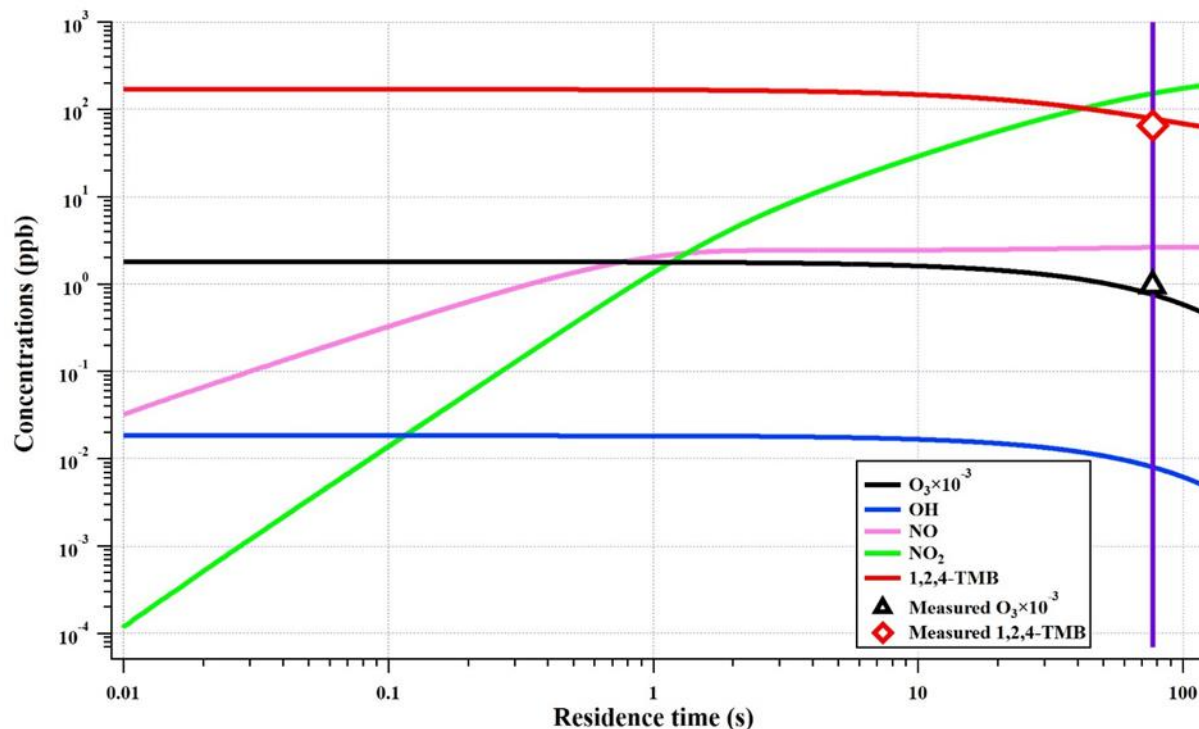


Figure R1. Modelled profiles by PAM_chem_v8 of different oxidants, NO_x and the precursor under the settings of “low NO_x experiment” (initial [O₃] = 1.8 ppm, initial [1,2,4-TMB] = 170 ppb, and irradiance of

254 nm Lamps = 2.0×10^{15} ph cm⁻² s). The measured [O₃] and [1,2,4-TMB] at the exit of OFR are shown by a triangle and a diamond, respectively, in the plot. The vertical purple line represents a residence time of 77.3 s.”

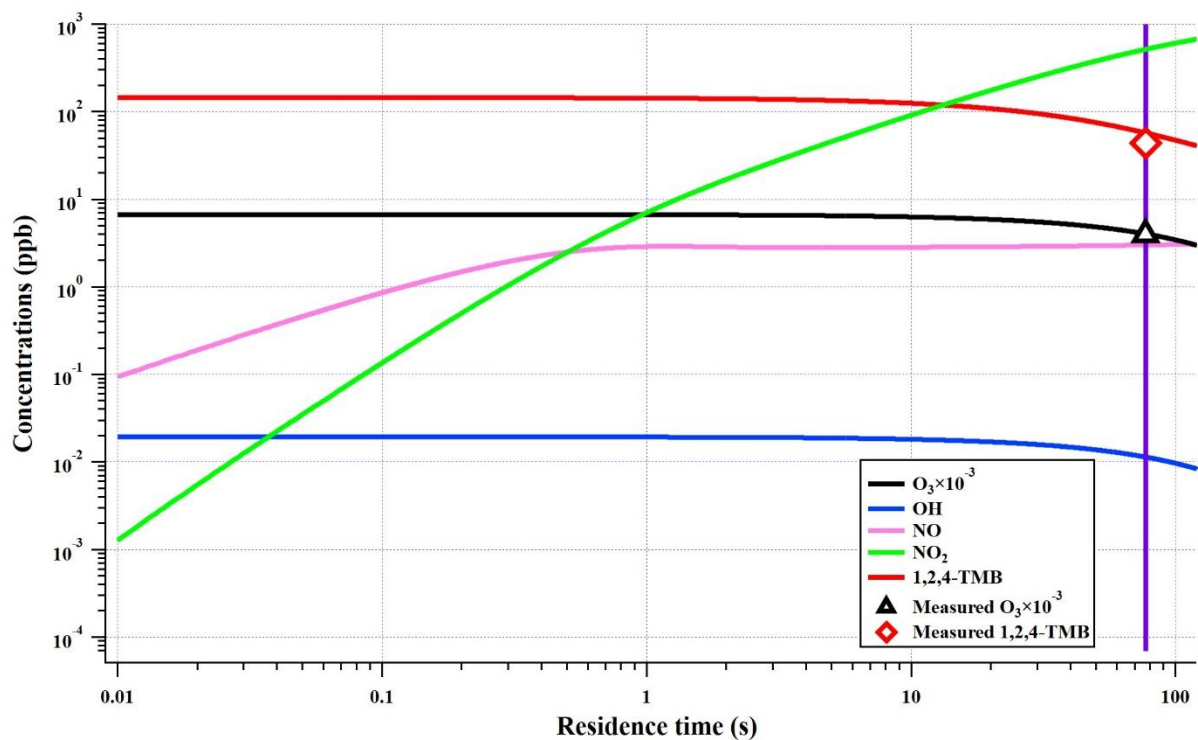


Figure R2. Modelled profiles by PAM_chem_v8 of different oxidants, NO_x and the precursor under the settings of “higher NO_x experiment” (initial [O₃] = 6.7 ppm, initial [1,2,4-TMB] = 145 ppb, and irradiance of 254 nm Lamps = 1.28×10^{15} ph cm⁻² s). The measured [O₃] and [1,2,4-TMB] at the exit of OFR are shown by a triangle and a diamond, respectively, in the plot. The vertical purple line represents a residence time of 77.3 s.”

To investigate this discrepancy, we recalibrated our NO_x monitor and performed a series of new experiments under experimental conditions similar to experiments #7 and #8 (Table R1), and generally observed a factor of two discrepancy between modelled and measured NO/NO₂ (Figure R3 and R4). The mean ratio of modelled-to-measured [NO] at the exit of OFR were 0.64 ± 0.04 and 0.98 ± 0.01 for Exp. #R1-R4 (low NO_x) and Exp. #R5-R8 (higher NO_x), respectively, whereas those of modelled-to-measured [NO₂] at the exit of OFR were 0.51 ± 0.07 and 0.73 ± 0.01 for Exp. #R1-R4 and Exp. #R5-R8, respectively. Hence, we reached a conclusion that our NO_x monitor malfunctioned during our previous experiments. Since the setting of mass spectrometers have altered significantly and thus the new mass spectrometric results are not directly comparable to those in previous experiment. We decide to keep the previous mass spectrometric results but report the modelled NO_x concentrations, which have no impacts on the conclusions of this study.

Table R1. Summary of experimental conditions for a series of new experiments carried out during the revision. The total flow was set to be 10.4 slpm and [N₂O] was the same as that in the previous experiments.

Exp. #R1-R4 correspond to Exp. #7 (low NO_x), and Exp. #R5-R8 correspond to Exp. #8 (high NO_x). In Exp. #R1-R4, the 254 nm lamps were tuned to get different NO/NO₂ levels and so were in Exp. #R5-R8. Reported [NO] and [NO₂] are values at the exit of OFR.

#	Precursor	Precursor concentration (ppb)	Consumption of precursor (%)	RH(%)	O ₃ concentration (ppb)	Measured NO(ppb)/NO ₂ (ppb)	Modelled NO(ppb)/NO ₂ (ppb)
R1	1,2,4-TMB	182	59.2	15.2	990	3.8/336.5	2.5/152.1
R2	1,2,4-TMB	191	51.7	15.2	1185	2.03/244.9	1.6/113.2
R3	1,2,4-TMB	205	60.2	15	868	5.38/360.6	3.2/185.0
R4	1,2,4-TMB	220	41.5	14.9	1342	1.17/178.1	1.1/84.1
R5	1,2,4-TMB	141	51.3	8.7	3953	3.2/791.8	3.1/550.9
R6	1,2,4-TMB	147	46.7	8.7	4671	1.8/528.2	1.7/365.1
R7	1,2,4-TMB	150	52.0	8.7	3375	4.5/1005.5	4.5/692.0
R8	1,2,4-TMB	155	52.9	8.5	2946	6.1/1079.9	6.0/854.1

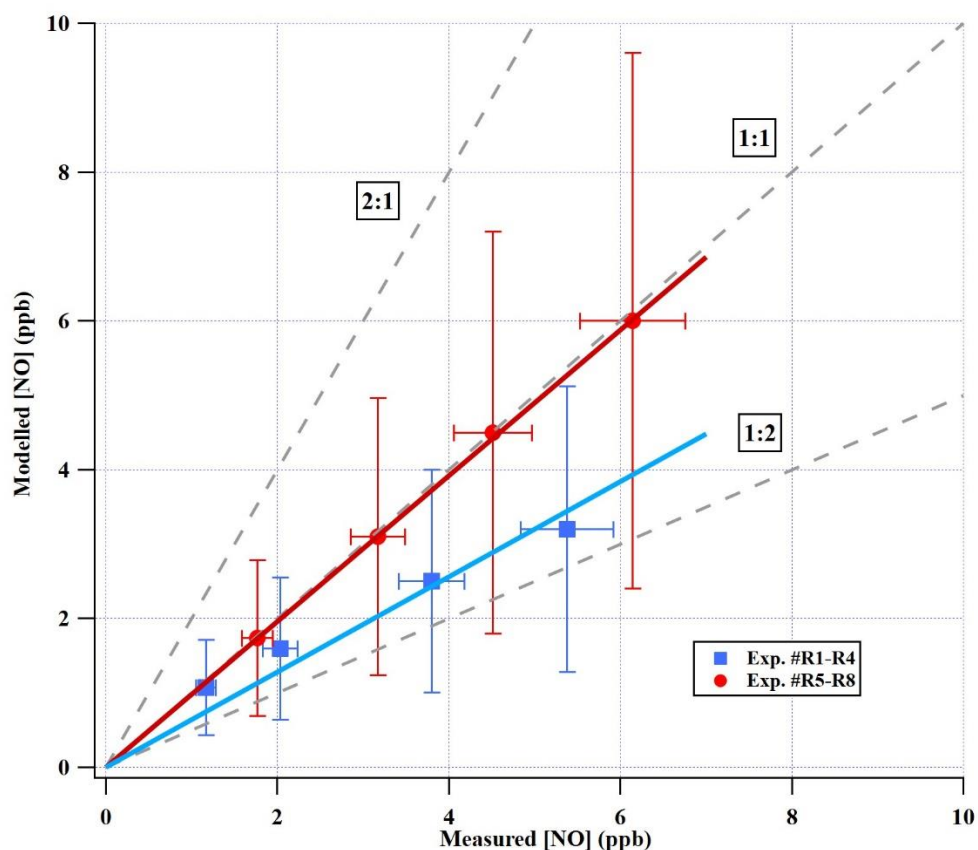


Figure R3. Measured *v.s.* modelled [NO] at a residence time of 77.3 s at the exit of the OFR. Error bars represent either $\pm 60\%$ uncertainty in model outputs (Peng et al., 2015) or $\pm 10\%$ precision in [NO] measurements by a calibrated NO_x monitor. The mean ratio of modelled-to-measured [NO] at the exit of OFR were 0.64 ± 0.04 and 0.98 ± 0.01 for Exp. #R1-R4 and Exp. #R5-R8, respectively.

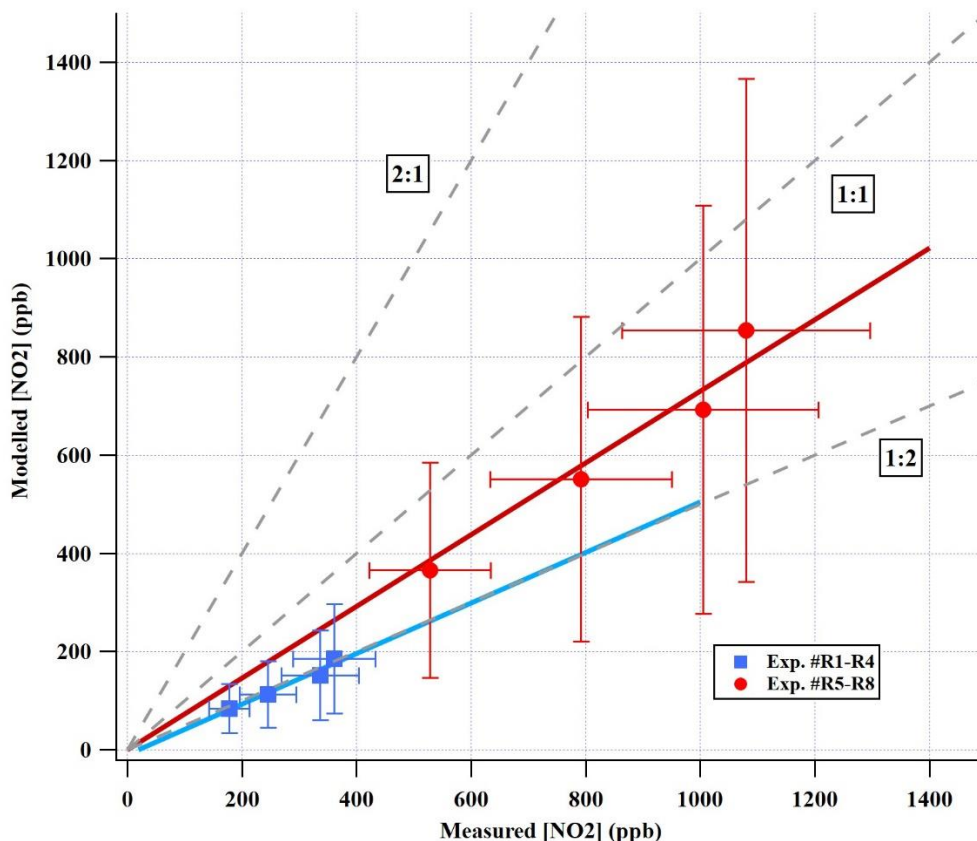


Figure R4. Measured *v.s.* modelled [NO₂] at a residence time of 77.3 s at the exit of the OFR. Error bars represent either $\pm 60\%$ uncertainty in model outputs (Peng et al., 2015) or $\pm 20\%$ precision in [NO₂] measurements by a calibrated NO_x monitor. The mean ratio of modelled-to-measured [NO₂] at the exit of OFR were 0.51 ± 0.07 and 0.73 ± 0.01 for Exp. #R1-R4 and Exp. #R5-R8, respectively.

We have now stated in our revised manuscript (Line 119-121) that “In addition, an ozone monitor (Model 106-M, 2B technologies) was utilized to measure ozone concentration, whereas a set of ...”,

(Line 127) that “approximately 80 seconds (77.3 seconds at 10.4 slpm)”,

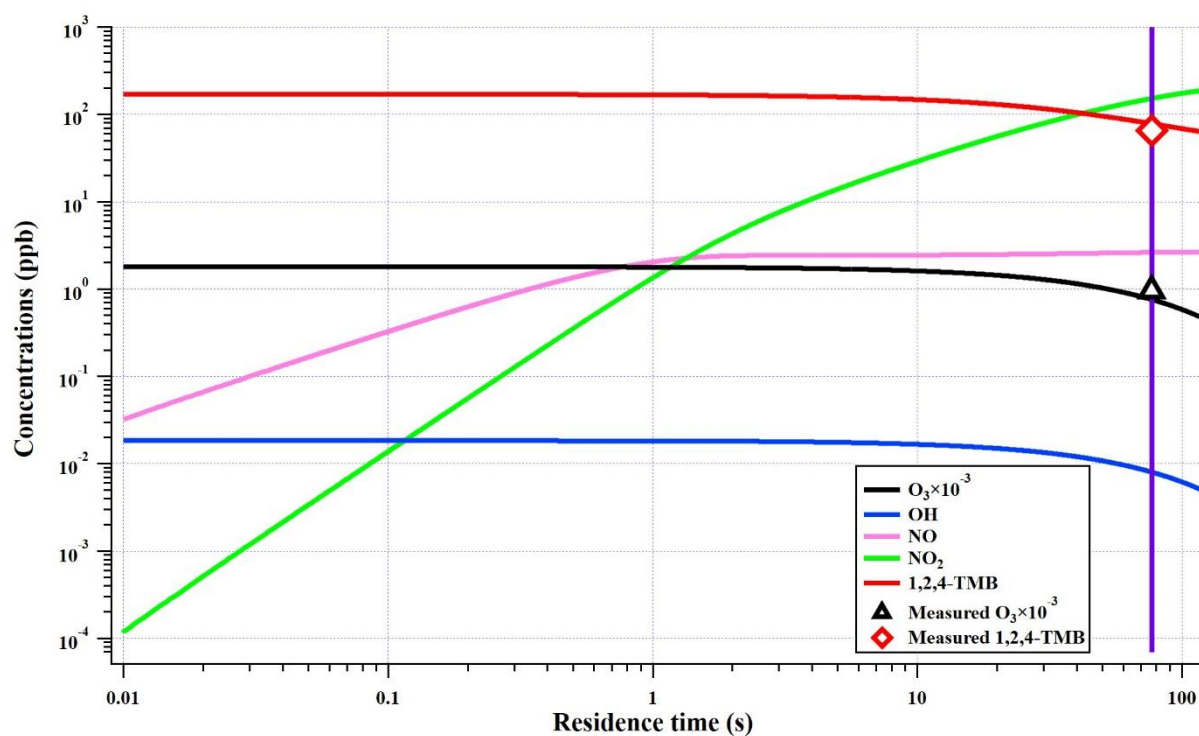
(Line 143-145) that “A photochemical model (PAM_chem_v8) (Lambe et al., 2017; Li et al., 2015; Peng et al., 2015) was implemented to constrain the NO/NO₂ profiles in the experiments, whose details are presented in Section S1”,

(Line 428-432) that “To constrain the NO_x level in the OFR, the profiles of NO/NO₂ were modelled by PAM_chem_v8, as shown in Figure S5. The mathematically-averaged NO_x levels in the low NO_x

experiment (Exp. #7) and higher NO_x experiment (Exp. #8) were 92 ppb (2.5 ppb NO + 89.5 ppb NO_2) and 295.3 ppb (2.9 ppb NO + 292.4 ppb NO_2), respectively. The NO_x/VOC in our experiments is comparable to ambient values in polluted areas. The $\text{NO}_x/(\Delta\text{VOC})$ was around 0.9 in the low NO_x experiment and 2.9 in the higher NO_x one.”

and (Section S1 in the supplement) that “Figure S5 shows the modelled profiles of the major oxidants, NO_x , and the precursor under the settings of Exp. #7 and Exp. #8 in Table 1. In the low NO_x experiment, the modelled $[\text{O}_3]$ is 20% lower than the measured value at the exit of OFR whereas the modelled [1,2,4-TMB] is 19% higher than the measured one. In the higher NO_x experiment, the modelled $[\text{O}_3]$ is 3% higher than the measured value whereas the modelled [1,2,4-TMB] is 23% higher than the measured one.

(a)



(b)

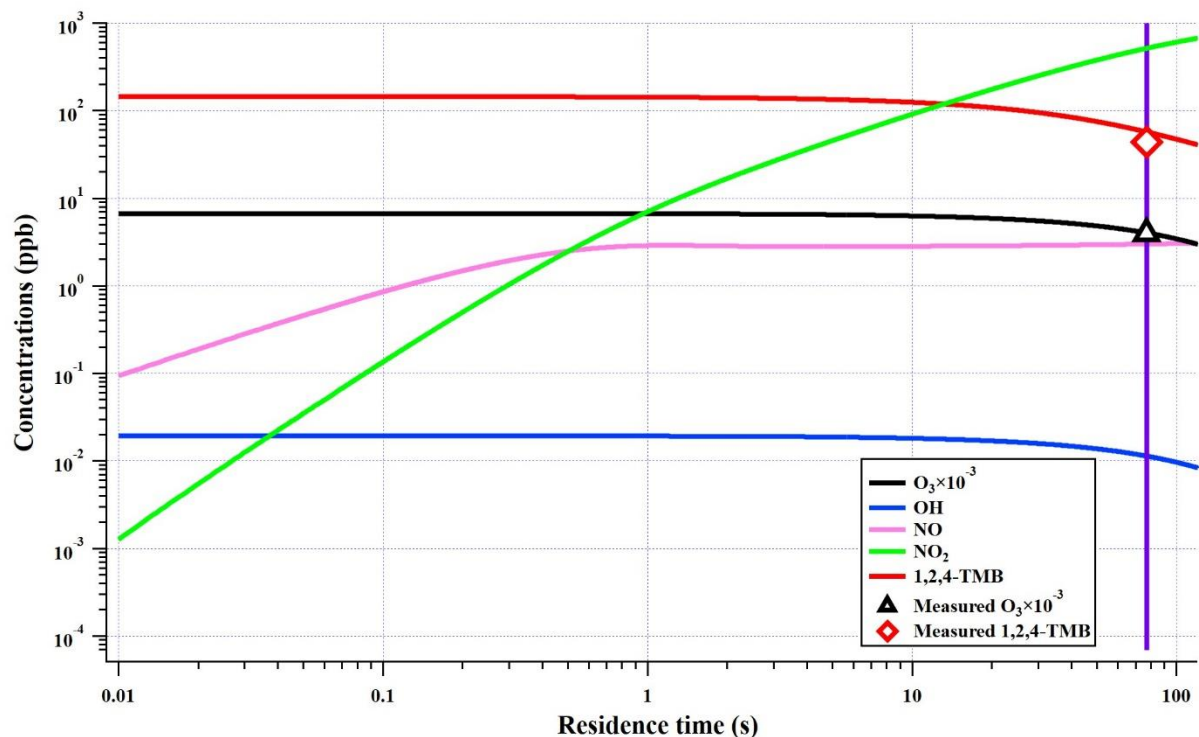


Figure S5. Modelled profiles by PAM_chem_v8 of different oxidants, NO_x and the precursor under the settings of (a) low NO_x experiment (initial [O₃] = 1.8 ppm, initial [1,2,4-TMB] = 170 ppb, and irradiance of 254 nm Lamps = 2.0×10^{15} ph cm⁻² s), and (b) higher NO_x experiment (initial [O₃] = 6.7 ppm, initial [1,2,4-TMB] = 145 ppb, and irradiance of 254 nm Lamps = 1.28×10^{15} ph cm⁻² s). The measured [O₃] and [1,2,4-TMB] at the exit of OFR are shown by a triangle and a diamond in the plot. The vertical purple line represents a residence time of 77.3 s.

The updated Table 1 is shown below

Table 1. Summary of experimental conditions.

#	Precursor	Experimental condition	Precursor concentration (ppb)	Consumption of precursor (%)	RH (%)	Total flow rate (slpm)	O ₃ concentration (ppb)
1	1,2,4-TMB	OH	158	59.3	12.5	10	712
2	1,3,5-TMB	OH	118	62.8	13.6	10	845
3	1,2,3-TMB	OH	214	58.4	8.1	10	1426
4	1,2,4-(1-methyl-D3)-TMB	OH	155	62.0	11.6	10	1003
5	1,2,4-(2-methyl-D3)-TMB	OH	169	61.8	12.5	10	776

6	1,2,4-(4-methyl-D3)-TMB	OH	166	62.8	11.5	10	886
7	1,2,4-TMB	Low NO _x (2.5 ppb NO + 89.5 ppb NO ₂) ^a	170	61.5	12.7	10.4	944
8	1,2,4-TMB	Higher NO _x (2.9 ppb NO + 292.4 ppb NO ₂) ^a	145	69.7	9.3	10.4	3911

^a Modelled mathematically-averaged NO/NO₂ concentrations in the OFR are shown here because of the malfunction of a NO_x monitor. The model underestimates [NO] and [NO₂] by up to a factor of 2, according to separate experiments that are not presented.

Lastly, the text in the Line 403-405 of the original manuscript that “The NO_x levels in the low NO_x experiment (Exp. #7) and higher NO_x experiment (Exp. #8) were 0.8 ppb and 6.5 ppb, respectively. Compared to the ambient values in polluted areas, this NO_x/VOC is low. The NO_x/(ΔVOC) was around 0.8% in the low NO_x experiment and 6.4% in higher NO_x one” have been deleted.

3. - Line 197 – 203: *From kinetic perspective, secondary chemistry, i.e. OH + product steps, cannot be neglected for a reactant conversion of 62.3 % in this system. What does it mean “one oxidation lifetime”?*

Response. The statement “under this condition, the production of the first-generation products is generally favored” does not exclude the possibility of secondary reactions. “One oxidation lifetime” means the concentration of the reactant decreases to 1/*e* of its initial concentration, i.e., consumption of 63.2% of the initial reactant. To clarify our points, we have now stated in our revised manuscript that (Line 204-208) “...so that the OH exposure in the OFR was close to one oxidation lifetime of TMB, i.e., consumption of (1-1/*e*) of the initial TMB. Under this condition, the production of the first-generation products is generally favored and the multi-generation products are also present, if the subsequent loss reactions for these products are assumed to proceed in the similar rate.”

Please also refer to our response to Comment #2 from Reviewer #1.

4. -Table 1: *The authors also used huge ozone concentrations in their runs, (1.7 – 9.6) ×10¹³ molecules cm⁻³. After first OH attack the trimethylbenzene loses its aromaticity forming a series of unsaturated closed-shell products. What about the possible ozonolysis of these products?*

Response. The significance of ozonolysis of these products can be estimated using the concentrations of ozone and OH, and the associated reaction rates with unsaturated closed-shell products. The decay of a VOC by reactions with OH/O₃ is defined as,

$$\frac{d[VOC]}{dt} = -k_{VOC+oxidant}[Oxidant][VOC]$$

where $k_{VOC+oxidant}$ is the reaction rates of VOC with OH/O₃. As a result, the lifetime of a VOC due to its reactions with OH/O₃ is defined as,

$$t_{OH} = \frac{1}{k_{VOC+oxidant}[Oxidant]}$$

Since the concentration of TMB can be measured online via Vocus PTR, we can determine the averaged OH radical concentration in the oxidation flow reactor according to the decay of TMB, whereas the concentration of O₃ can be measured with an O₃ box.

Now let's take the 1,3,5-TMB + OH experiment for example, where [OH] = 2.2×10^8 molecules cm⁻³, and [O₃] = 2.11×10^{13} molecules cm⁻³. No systematic research has been performed on the reaction rate of ozone with the first-generation oxidation products of trimethylbenzene. However, the reaction rates for ozonolysis of VOCs typically range from 10^{-16} to 10^{-18} cm³ molecules⁻¹ s⁻¹. A distinct feature of the aromatic oxidation is the faster oxidation rates of the first-generation products as compared to the parent molecule (Garmash et al., 2020). The pi-electron structure of the aromatic ring makes the parent molecule less susceptible towards OH oxidation compared to most organic molecules. It is thus assumed that the reaction rate between OH and the typical bicyclic first-generation product is $\sim 1.5 \times 10^{-10}$ molecules cm⁻³ (MCM v3.3.1, available at: <http://mcm.leeds.ac.uk/MCM>). Therefore, we can determine the lifetimes of unsaturated closed-shell products against OH and ozone, respectively.

$$\begin{aligned} t_{OH} &= 30.3 \text{ s} \\ t_{O_3} &= 473.9 \sim 47393.3 \text{ s} \end{aligned}$$

Hence, ozonolysis is not expected to be a significant reaction route in our system, which is consistent with a former study (Molteni et al., 2018). Also, Berndt et al. (2018) show that the formation of ROOR' accretion products from TMB is a pure RO₂+R'O₂ gas-phase reaction without any hidden effects exerted by ozonolysis.

5. - *Schemes: It should be clarified what the authors mean with “stabilized products”.*

Response. Here, the term “stabilized products” refers to “non-radical products”, which shows up for a lot of times in the manuscript. On the other hand, several researchers used “closed-shell products”, which we prefer not to use. We have revised our manuscript and added a clarification at the position where this term shows up for the first time (Line 96 - 97):” Subsequent reactions of the intermediates will lead to the formation of stabilized products (or non-radical products),”

6. - *Figure 5: A C₁₈ product fraction of more than 50% is very surprising for me. This finding should be discussed in respect of rates of the competing steps R5 – R8.*

Response. In fact, our study is not the first one that observed a dimer product fraction of more than 50%, as mentioned in Line 377-379 from the previous version of manuscript. It is likely a result from the high

precursor concentrations and should not be implied to the ambient as discussed in our response to the general comment from Reviewer #2.

We have now stated in our manuscript that (Line 393-417) “In the 1,3,5-TMB oxidation experiments (Exp. #2), where the highest C18 dimer fraction was observed, the mole fraction of the C18 dimers is likely determined by the competition of reactions R5, R6, R7, and R8, which can be mathematically expressed as

$$f_{C18} = \frac{0.5 \times k_{R8}[RO_2]}{k_{R5,R6}[RO_2] + k_{R7}[HO_2] + 0.5 \times k_{R8}[RO_2]} \quad (1)$$

where $k_{R5,R6}$ stands for the reaction rates for R5 and R6, assumed to be around $8.8 \times 10^{-13} \text{ cm}^3 \text{ molecule}^{-1} \text{ s}^{-1}$ by MCM, k_{R7} is the reaction rate for R7, set at a typical value of $2 \times 10^{-11} \text{ cm}^3 \text{ molecule}^{-1} \text{ s}^{-1}$ (Berndt et al., 2018b; Bianchi et al., 2019), and k_{R8} is the reaction rate of R8 for BPRs generated by 1,3,5-TMB, which has recently been measured to be as fast as $10^{-10} \text{ cm}^3 \text{ molecule}^{-1} \text{ s}^{-1}$ (Berndt et al., 2018b).

Since the concentration of HO_2 in the OFR was not measured, we utilized a kinetic reaction model (PAM_chem_v8) to characterize the concentration profiles of oxidants in the OFR, which include OH, O_3 , HO_2 , and H_2O_2 . A detailed description of this model is given in section S1 of the supplement and the modelled profiles of oxidants and precursors are shown in Figure S4. According to the model, the steady-state concentration of HO_2 in the Exp. #2 was around 18 ppt ($\sim 4.5 \times 10^8 \text{ molecules cm}^{-3}$). On the other hand, it is difficult to evaluate the effective concentration of the RO_2 radicals in the system, because RO_2 with low oxidation states will not form HOMs via reactions R5-R8. Therefore, we estimated the concentration of RO_2 in Eq. (1) to be close to that of BPRs in the OFR. According to MCM v3.3.1, the branching ratio for the peroxide-bicyclic pathway in the OH oxidation of 1,3,5-TMB is 79%, so that the concentration of BPRs was roughly estimated to be 58.5 ppb ($\sim 1.5 \times 10^{12} \text{ molecules cm}^{-3}$, 79% of the reacted 1,3,5-TMB). Hence, the fraction of C18 dimer is estimated to be around 98%. Clearly, this estimation itself comes with a large uncertainty, and the estimated fraction can only be regarded as an indication of explainable high yields of C18 dimers instead of a rigorous number.

In fact, under our experimental conditions, the C18 dimer fraction in the 1,3,5-TMB experiments was around 86.5%, which is much higher than the dimer fraction of 42.6%-56.5% re-calculated using the measured C9 and C18 signals by Tsiligiannis et al. (2019), 43.3%-52.4% modelled by Tsiligiannis et al. (2019), and 39% reported by Molteni et al. (2018).”,

and in Section S1 of the supplement that “PAM_chem_v8 is a model developed in conjunction with the PAM, which includes the chemistry of photolysis of oxygen, water vapor, and other trace gases by the primary wavelengths in mercury lamps (254 nm and 185 nm) (Lambe et al., 2017; Li et al., 2015; Peng et al., 2015). Simplified VOC and RO_2 chemistry are also included, but the first-generation stabilized products and the second-generation organic radical products do not react further in the model.

Fig S4 shows the modelled concentration profiles of different oxidants and 1,3,5-TMB with an irradiance of 1.64×10^{15} ph cm⁻² s by 254 nm lamps. The initial concentrations of O₃ ([O₃]) (1.2 ppm) and 1,3,5-TMB ([1,3,5-TMB]) were measured before turning on the 254 nm lamps. [O₃] and [1,3,5-TMB] at an 80 s residence time were also measured. The modelled [O₃] is 20% lower than the measured value whereas modelled [1,3,5-TMB] is very close (4% higher) to the measured one, which shows the reliability of this model.

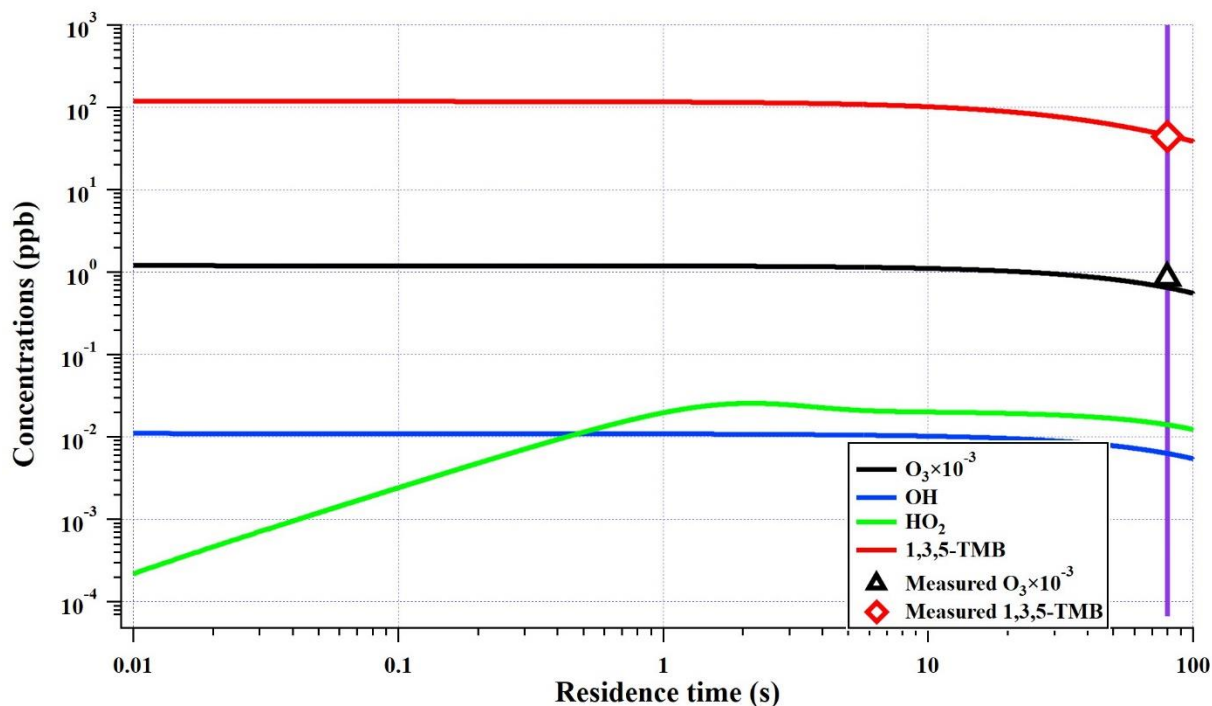


Figure S4. Concentration profiles of different oxidants and 1,3,5-TMB outputted by PAM_chem_v8 under the settings of Exp. #2. Initial [O₃] and [1,3,5-TMB] are 1.2 ppm and 118 ppb, respectively, which were used as input of the model. The measured [O₃] and [1,3,5-TMB] at the exit of OFR are shown by a triangle and a diamond, respectively. Input of irradiance of 254 nm lamps, I_{254} , is 1.64×10^{15} ph cm⁻² s, which was measured with a photodiode in the OFR. The vertical purple line represents a residence time of 80 s”

References:

- Berndt, T., Scholz, W., Mentler, B., Fischer, L., Herrmann, H., Kulmala, M. and Hansel, A.: Accretion Product Formation from Self- and Cross-Reactions of RO₂ Radicals in the Atmosphere, *Angew. Chemie Int. Ed.*, 57(14), 3820–3824, doi:10.1002/anie.201710989, 2018.
- Ehn, M., Thornton, J. A., Kleist, E., Sipilä, M., Junninen, H., Pullinen, I., Springer, M., Rubach, F., Tillmann, R., Lee, B., Lopez-Hilfiker, F., Andres, S., Acir, I. H., Rissanen, M., Jokinen, T., Schobesberger, S., Kangasluoma, J., Kontkanen, J., Nieminen, T., Kurtén, T., Nielsen, L. B., Jørgensen, S., Kjaergaard, H. G., Canagaratna, M., Maso, M. D., Berndt, T., Petäjä, T., Wahner, A., Kerminen, V. M., Kulmala, M., Worsnop, D. R., Wildt, J. and Mentel, T. F.: A large source of low-volatility secondary organic aerosol, *Nature*, 506(7489), 476–479, doi:10.1038/nature13032, 2014.
- Garmash, O., Rissanen, M. P., Pullinen, I., Schmitt, S., Kausiala, O., Tillmann, R., Zhao, D., Percival, C., Bannan, T. J., Priestley, M., Hallquist, Å. M., Kleist, E., Kiendler-Scharr, A., Hallquist, M., Berndt, T., McFiggans, G., Wildt, J., Mentel, T. F. and Ehn, M.: Multi-generation OH oxidation as a source for highly oxygenated organic molecules from aromatics, *Atmos. Chem. Phys.*, 20(1), 515–537, doi:10.5194/acp-20-515-2020, 2020.
- de Gouw, J. and Warneke, C.: Measurements of volatile organic compounds in the earth's atmosphere using proton-transfer-reaction mass spectrometry, *Mass Spectrom. Rev.*, 26(2), 223–257, doi:10.1002/mas.20119, 2007.
- Gueneron, M., Erickson, M. H., Vanderschelden, G. S. and Jobson, B. T.: PTR-MS fragmentation patterns of gasoline hydrocarbons, *Int. J. Mass Spectrom.*, 379, 97–109, doi:10.1016/j.ijms.2015.01.001, 2015.
- Hyttinen, N., Kupiainen-Määttä, O., Rissanen, M. P., Muuronen, M., Ehn, M. and Kurtén, T.: Modeling the Charging of Highly Oxidized Cyclohexene Ozonolysis Products Using Nitrate-Based Chemical Ionization, *J. Phys. Chem. A*, 119(24), 6339–6345, doi:10.1021/acs.jpca.5b01818, 2015.
- Karl, T., Striednig, M., Graus, M., Hammerle, A. and Wohlfahrt, G.: Urban flux measurements reveal a large pool of oxygenated volatile organic compound emissions, *Proc. Natl. Acad. Sci. U. S. A.*, 115(6), 1186–1191, doi:10.1073/pnas.1714715115, 2018.
- Lambe, A., Massoli, P., Zhang, X., Canagaratna, M., Nowak, J., Daube, C., Yan, C., Nie, W., Onasch, T., Jayne, J., Kolb, C., Davidovits, P., Worsnop, D. and Brune, W.: Controlled nitric oxide production via O(1D) + N₂O reactions for use in oxidation flow reactor studies, *Atmos. Meas. Tech.*, 10(6), 2283–2298, doi:10.5194/amt-10-2283-2017, 2017.
- Li, R., Palm, B. B., Ortega, A. M., Hlywiak, J., Hu, W., Peng, Z., Day, D. A., Knote, C., Brune, W. H., De Gouw, J. A. and Jimenez, J. L.: Modeling the radical chemistry in an oxidation flow reactor: Radical formation and recycling, sensitivities, and the OH exposure estimation equation, *J. Phys. Chem. A*, 119(19), 4418–4432, doi:10.1021/jp509534k, 2015.
- Molteni, U., Bianchi, F., Klein, F., Haddad, I. El, Frege, C., Rossi, M. J., Dommen, J. and Baltensperger, U.: Formation of highly oxygenated organic molecules from aromatic compounds, *Atmos. Chem. Phys.*, 18, 1909–1921, doi:10.5194/acp-18-1909-2018, 2018.
- Peng, Z. and Jimenez, J. L.: Radical chemistry in oxidation flow reactors for atmospheric chemistry research, *Chem. Soc. Rev.*, 49(9), 2570–2616, doi:10.1039/c9cs00766k, 2020.
- Peng, Z., Day, D. A., Stark, H., Li, R., Lee-Taylor, J., Palm, B. B., Brune, W. H. and Jimenez, J. L.: HO_x radical chemistry in oxidation flow reactors with low-pressure mercury lamps systematically examined by modeling, *Atmos. Meas. Tech.*, 8, 4863–4890, doi:10.5194/amt-8-4863-2015, 2015.
- Peng, Z., Palm, B. B., Day, D. A., Talukdar, R. K., Hu, W., Lambe, A. T., Brune, W. H. and Jimenez, J. L.: Model Evaluation of New Techniques for Maintaining High-NO Conditions in Oxidation Flow Reactors for the Study of OH-Initiated Atmospheric Chemistry, *ACS Earth Sp. Chem.*, 2(2), 72–86, doi:10.1021/acsearthspacechem.7b00070, 2018.
- Španěl, P. and Smith, D.: On the features, successes and challenges of selected ion flow tube mass spectrometry, *Eur. J. Mass Spectrom.*, doi:10.1255/ejms.1240, 2013.
- Tani, A.: Fragmentation and reaction rate constants of terpenoids determined by proton transfer reaction-mass spectrometry, *Environ. Control Biol.*, 51(1), 23–29, doi:10.2525/ecb.51.23, 2013.

Yuan, B., Koss, A. R., Warneke, C., Coggon, M., Sekimoto, K. and De Gouw, J. A.: Proton-Transfer-Reaction Mass Spectrometry: Applications in Atmospheric Sciences, *Chem. Rev.*, 117(21), 13187–13229, doi:10.1021/acs.chemrev.7b00325, 2017.

Oxygenated products formed from OH-initiated reactions of trimethylbenzene: Autoxidation and accretion

Yuwei Wang¹, Archit Mehra², Jordan E. Krechmer³, Gan Yang¹, Xiaoyu Hu¹, Yiqun Lu¹, Andrew Lambe³, Manjula Canagaratna³, Jianmin Chen¹, Douglas Worsnop³, Hugh Coe², Lin Wang^{1,4,5} *

¹ Shanghai Key Laboratory of Atmospheric Particle Pollution and Prevention (LAP³), Department of Environmental Science and Engineering, Jiangwan Campus, Fudan University, Shanghai 200438, China

² Centre for Atmospheric Science, School of Earth and Environment Sciences, The University of Manchester, Manchester, M13 9PL, UK

³ Center for Aerosol and Cloud Chemistry, Aerodyne Research Inc., Billerica, MA, USA

⁴ Collaborative Innovation Center of Climate Change, Nanjing 210023, China

⁵ Shanghai Institute of Pollution Control and Ecological Security, Shanghai 200092, China

* Corresponding Author: L.W., email, lin_wang@fudan.edu.cn; phone, +86-21-31243568

Abstract. Gas-phase oxidation pathways and products of anthropogenic volatile organic compounds (VOCs), mainly aromatics, are the subject of intensive research with attention paid to their contributions to secondary organic aerosol (SOA) formation and potentially, new particle formation (NPF) in the urban atmosphere. In this study, a series of OH-initiated oxidation experiments of trimethylbenzene (TMB, C₉H₁₂) including 1,2,4-TMB, 1,3,5-TMB, 1,2,3-TMB, and 1,2,4-(methyl-D₃)-TMBs (C₉H₉D₃) were investigated in an oxidation flow reactor (OFR), in the absence and presence of NO_x. Products were measured using a suite of state-of-the-art instruments, i.e., a nitrate-based chemical ionization - atmospheric pressure interface time-of-flight mass spectrometer (Nitrate CI-API-TOF), an iodide-adduct chemical ionization - time-of-flight mass spectrometer (Iodide CI-TOF) equipped with a Filter Inlet for Gases and AEROSols (FIGAERO), and a Vocus proton-transfer-reaction mass spectrometer (Vocus PTR). A large number of C₉ products with 1-11 oxygen atoms and C₁₈ products presumably formed from dimerization of C₉ peroxy radicals were observed, hinting the extensive existence of autoxidation and accretion reaction pathways in the OH-initiated oxidation reactions of TMBs. Oxidation products of 1,2,4-(methyl-D₃)-TMBs with deuterium atoms in different methyl substituents were then used as a molecular basis to propose potential autoxidation reaction pathways. Accretion of C₉ peroxy radicals is the most significant for aromatics with meta-substituents and the least for aromatics with ortho-substituents, if the number and size of substituted groups are identical. The presence of NO_x would suppress the formation of C₁₈ highly oxygenated molecules (HOMs) and enhance the formation of organonitrates, and even dinitrate organic compounds. Our results show that the oxidation products of TMB are much more diverse and could be more oxygenated than the current mechanisms predict.

1 Introduction

Oxidation products of volatile organic compounds (VOCs) contribute significantly to the formation of secondary organic aerosols (SOAs) (Ng et al., 2010; Zhang et al., 2007), which raises a globally ubiquitous health and environmental concern (Hallquist et al., 2009). There have been numerous studies that aim to construct detailed VOC oxidation mechanisms to advance our understanding on VOC degradation, SOA formation, and ozone formation (Atkinson, 1986; Atkinson and Arey, 2003; Atkinson and Carter, 1984; Kroll and Seinfeld, 2008; Ziemann and Atkinson, 2012). Based on the hypothesis that the products and

kinetics of many unstudied chemical reactions can be proposed by analogy to known reactions of similar chemical species (Ziemann and Atkinson, 2012) and/or predicted by the structure-activity relationships (Kwok and Atkinson, 1995), the Master Chemical Mechanism (MCM) is developed as a nearly explicit chemical mechanism, describing the degradation of numerous VOCs (Bloss et al., 2005; Jenkin et al., 2003; Saunders et al., 2003). Due to the high complexity of VOC oxidation processes, it is not surprising that mechanisms leading to the formation of previously unidentified species are still missing.

The formation of highly oxygenated organic molecules (HOMs) through the autoxidation pathway during VOC oxidation is such an example. HOMs refer to organic compounds typically containing six or more oxygen atoms that are formed in the gas phase (Bianchi et al., 2019). Autoxidation is a chemical process where an alkyl peroxy radical (RO_2) undergoes an intramolecular hydrogen shift followed by addition of a molecular oxygen, resulting in a more oxygenated RO_2 radical (Crounse et al., 2013; Ehn et al., 2014). It is an effectively repetitive uni-molecular reaction as the more oxidized RO_2 will serve as a parent RO_2 in the next autoxidation reaction, leading to the rapid formation of HOMs in very short time scales (Bianchi et al., 2019; Jørgensen et al., 2016).

Owing to recent developments in the analytical techniques such as nitrate-anion chemical ionization mass spectrometry (nitrate CIMS), our knowledge on the autoxidation pathway during the oxidation of biogenic volatile organic compounds (BVOCs) has been significantly improved. Certain systems, such as the oxidation of monoterpenes, have been studied extensively, of which ozonolysis has been confirmed as an important source for HOMs (Ehn et al., 2014; Jokinen et al., 2014). The OH-initiated oxidation is also a considerable HOM formation source for monoterpenes and isoprene (Krechmer et al., 2015), albeit at lower yields for monoterpenes containing an endocyclic double bond (Jokinen et al., 2014, 2015; Rissanen et al., 2015). Detailed mechanisms of monoterpene-derived HOM formation reactions, initiated by ozone or OH, were investigated through theoretical calculations (Berndt et al., 2016), or by analogy to reactions of similar chemical species, i.e., cyclohexene (Rissanen et al., 2014). A couple of studies performed H/D isotope exchange experiments, which can probe the number of hydrogen atoms other than that in C-H, strongly supporting the proposal of autoxidation mechanisms (Ehn et al., 2014; Rissanen et al., 2014). Research on other BVOCs, i.e., isoprene and sesquiterpenes (Crounse et al., 2013; Richters et al., 2016; Teng et al., 2017), and on other oxidants, i.e., NO_3 and chlorine (Nah et al., 2016; Wang et al., 2019), indicate the widespread existence of autoxidation pathways in the oxidation of BVOCs. The products formed from autoxidation of biogenic precursors have been proven to play a vital role in atmospheric new particle formation (NPF) because of their low volatility (Ehn et al., 2014; Stolzenburg et al., 2018; Tröstl et al., 2016).

On the other hand, studies on autoxidation of anthropogenic VOCs are rather sparse. Wang et al. (2017) theoretically and experimentally showed the autoxidation route of alkylbenzenes to form HOMs in the gas phase. Identities and yields of HOM products from different aromatics were systematically measured and the determined molar HOM yields were in the range of 0.1 % to 2.5 %, which are similar to the molar HOM yields of OH-initiated reactions of BVOCs (Jokinen et al., 2015; Molteni et al., 2018). Currently, aromatics-derived HOMs are believed to be formed via many reaction pathways, including accretion, bicyclic intermediate reactions, and multi-generation OH reactions (Berndt et al., 2018b; Garmash et al., 2019; Zaytsev et al., 2019). The unimolecular isomerization and autoxidation reactions of aromatic peroxy

radicals have been shown to be fast enough to compete with other bimolecular reactions even under NO concentrations as high as in urban environment (Tsiligiannis et al., 2019).

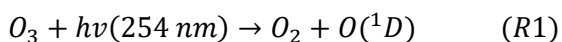
Trimethylbenzene (TMB) including isomers of 1,3,5-TMB, 1,2,3-TMB, and 1,2,4-TMB is one of the most common anthropogenic VOCs in urban areas. OH-initiated oxidation of TMB is its dominant chemical loss in the atmosphere (Atkinson and Arey, 2003), which proceeds either via H atom abstraction from the methyl substituents or via addition of OH radical onto the aromatic ring (Ziemann and Atkinson, 2012). The H atom abstraction channel is minor in the OH-induced oxidation reactions of TMB, forming dimethylbenzaldehyde. The major channels of OH addition consist of peroxide-bicyclic pathway, phenolic pathway, and epoxy-oxy pathway (Bloss et al., 2005; Calvert et al., 2002; Jenkin et al., 2003). The three TMB isomers have different branching ratios for these pathways resulting from the substitution-, site-, and stereo-specificity, however specific branching ratios are still in debate. Among these pathways, the peroxide-bicyclic pathway has the highest branching ratio and can form bicyclic peroxy radicals (BPRs), which are important intermediates that contribute significantly to the formation of HOMs (Wang et al., 2017). Subsequent reactions of the intermediates will lead to the formation of stabilized products (or non-radical products). On the other hand, the details of the autoxidation mechanisms for anthropogenic precursors remain elusive. Direct measurements of individual H-shift rates, the detailed structure of HOMs, and a robust quantification of HOM yields are still lacking. The detailed kinetics for termination reactions of different RO₂ are also ambiguous. Consequently, it is hard to comprehensively judge the TMB oxidation reaction pathways and products under different atmospheric conditions, and to evaluate the contribution of TMB oxidation to atmospheric NPF and SOA formation.

In this study, we studied the OH-initiated oxidation of 1,3,5-TMB, 1,2,3-TMB, and 1,2,4-TMB with a focus on autoxidation and accretion products, via the concurrent usage of a Vocus proton-transfer-reaction time-of-flight mass spectrometry (Vocus PTR), an iodide-adduct chemical ionization - time-of-flight mass spectrometer equipped with a Filter Inlet for Gases and AEROSols (FIGAERO Iodide CI-TOF), and a nitrate-based chemical ionization - atmospheric pressure interface time-of-flight mass spectrometer (Nitrate CI-APi-TOF). Oxidation of 1,2,4-(methyl-D3)-TMBs was investigated to elucidate the detailed autoxidation reaction pathway. The influence of NO_x concentration on product distribution was also investigated.

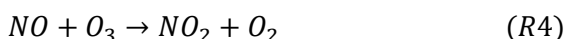
2 Methods

As shown in Figure 1, oxidation experiments of TMB were conducted in a Potential Aerosol Mass (PAM) oxidation flow reactor (OFR, Aerodyne Research, Inc.). A self-prepared VOC cylinder was used to provide a constant source of gaseous TMB as a reactant. O₃/OH was produced in-situ in the PAM and the relative humidity (RH) was regulated by the PAM setup, which will be introduced in details later. A Vocus PTR (Krechmer et al., 2018), a FIGAERO Iodide CI-TOF (Lee et al., 2014; Lopez-Hilfiker et al., 2014), and a Nitrate CI-APi-TOF (Ehn et al., 2014; Eisele and Tanner, 1993) were deployed to detect gaseous products as well as particulate ones. In addition, an ozone monitor (Model 106-M, 2B technologies) ~~and a NO_x monitor (Model 42i TLE; Thermo Fisher Scientific) were was~~ utilized to measure ~~trace gas concentration~~ ozone concentration, whereas a set of Scanning Mobility Particle Sizer (SMPS, consisting of one TSI Model 3080 Long DMA and one TSI Model 3776 Condensation Particle Counter) was employed to measure the number size distribution of submicron aerosol particles.

OFR. In this study, the sum of all the flows in the PAM, including a zero air flow, an ozone (O₃) flow, a TMB/N₂ flow, and a N₂O/N₂ flow depending upon experimental conditions, was kept at either 10 or 10.4 slpm (standard litres per minute, standard to 0 °C, 1 atm), resulting in calculated mean residence times of approximately 80 seconds (77.3 seconds at 10.4 slpm). Zero air was generated by a zero gas generator (Sabio Model 1001 Zero Gas Source). A fraction of the zero air was passed through a Nafion humidifier (Perma Pure Model FC100-80-6MSS) filled with ultrapure water to achieve the desired RH in the OFR. Ozone was generated by passing 800 sccm (standard cubic centimetre, standard to 0 °C, 1 atm) of zero air through a separate ozone chamber and input into the OFR. In order to create a low HO₂/RO₂ ratio environment to promote the carbonyl and hydroxyl channels to terminate RO₂ radicals, the OFR was operated with only the 254 nm lights on (Lambe et al., 2019), which is referred to as OFR254 mode in previous studies (Peng et al., 2015). In OFR254 mode, the primary oxidant production reactions in the OFR are:



In some experiments, N₂O (99.999%, Air Liquide) was added at the OFR inlet, corresponding to mixing ratios of 3.4% of the total gas flow rates, which produced NO_x via the following reactions (Lambe et al., 2017):



A photochemical model (PAM_chem_v8) (Lambe et al., 2017; Li et al., 2015; Peng et al., 2015) was implemented to constrain the NO/NO₂ profiles in the experiments, whose details are presented in Section S1.

Before each experiment, the PAM OFR was purged with zero air under the OFR254 operation mode until the signals of acetic acid and other common VOC oxidation products decreased to background levels of the Vocus PTR and CI-TOF that are described below.

Vocus PTR. The newly developed Vocus PTR has a high sensitivity to a wide range of VOCs and oxygenated volatile organic compounds (OVOCs) (Krechmer et al., 2018; Li et al., 2019; Riva et al., 2019). Its mass resolving power ($m/\Delta m = \sim 12000$ at 200 Th, 1 Th = 1 u/e , where e is the elementary charge and u is the atomic mass unit) allows to simultaneously monitor many isobaric species, and even to distinguish the very minor mass discrepancy (0.001548 u) between one deuterium atom and two hydrogen atoms. The instrument background together with a quantitative calibration by injection of standards was measured between every two experiments to minimize potential inaccuracies. In our study, the pressure of the focusing ion-molecule reactor (FIMR) was actively maintained at 1.5 mbar resulting in an E/N of the FIMR at 110 Td (1 Td = 1×10^{-17} V cm²), which was generally a moderate operating condition leading to relatively little fragmentation of compounds of interest (Gueneron et al., 2015; Yuan et al., 2017).

FIGAERO-Iodide CI-TOF. The Iodide-adduct CI-TOF is able to determine elemental compositions of a suite of atmospheric oxygenated organic species (D'Ambro et al., 2017; Lee et al., 2014; Lopez-Hilfiker et al., 2016). It has increasing sensitivities toward more polar and acidic VOCs (Lee et al., 2014). The mass resolution of the Iodide CI-TOF was tuned to be around 3000. The reagent ion (I⁻) was produced from permeated CH₃I vapor in N₂ by a radioactive source of Am-241 (0.1 mCi). The pressure in the ion-molecule

reactor (IMR) was regulated at 100 mbar, whereas the small segmented quadrupole (SSQ) pressure was set to be around 2 mbar. The FIGAERO inlet manifold enables the Iodide CI-TOF to measure both gas and particle compositions at a molecular level (Lopez-Hilfiker et al., 2014). In our study, aerosols were collected onto a PTFE filter (5 μ m, Millipore) at 0.96 slpm for 20 min, while the gases were measured simultaneously via a separate dedicated port. Then, a thermal desorption cycle was started 2 minutes after the FIGAERO filter was aligned to a heating tube, through which a heated ultra-high purity nitrogen flow was passed and heated according to a pre-programmed temperature ramp. The ultra-high purity nitrogen was initially held at 25 °C for 2 min, and then heated at a rate of 10 °C min⁻¹ to 200 °C, which was maintained for the remainder of the temperature ramp (50 min in total).

Nitrate CI-API-TOF. The Nitrate CI-API-TOF has been increasingly used for the measurement of low volatility organic compounds (LVOC) and extremely low volatility organic compounds (ELVOCs) (Ehn et al., 2014; Hyttinen et al., 2015; Jokinen et al., 2014), which mostly have a high O:C ratio. The resolving power of the Nitrate CI-API-TOF was up to around 8000 in our study. The selectivity of nitrate ions keeps the spectrum clean from the more abundant, less oxidized compounds in our experiments. Most of the detected species were observed exclusively as adducts with NO₃⁻, a very minor fraction of which contain odd hydrogen numbers and are hence postulated to be radicals but not presented in this manuscript.

The concurrent use of three mass spectrometers (MSs) with different reagent ions allows us to obtain a comprehensive picture of the oxidation products of TMB with OH radicals. The detection suitability of these three instruments for oxidation products with various levels of oxidation has been discussed a lot in previous studies (Isaacman-VanWertz et al., 2017; Krechmer et al., 2018; Riva et al., 2019). Generally, Vocus PTR displays selectivity for less oxidized compounds; Iodide CI-TOF favors more oxygenated species; and Nitrate CI-API-TOF shows the highest efficiency for the most oxidized compounds. Dimer products of TMB oxidation are expected to be detected by Nitrate CI-API-TOF as clusters with NO₃⁻, which is due to the potential hydrogen bond donor functional groups in these molecules, inferred from the abundant oxygen and hydrogen atoms in the formulas. These products should not be detected by Vocus PTR. One explanation is that these molecules are likely to be fragile and therefore have fragmented owing to the protonation or the strong electric field in the FIMR of Vocus PTR. Alternatively, these products might not go through the PEEK tube inlet of Vocus PTR. At the same time, the sample inlet for Iodide CI-TOF in our experiments is not desirable for the detection of dimer products.

To ensure that the reported signal is truly from the sample flow instead of internal background or contamination, subtraction of the mass spectra for the OFR background from the samples has been performed for each instrument. In addition, since this study is mostly concerned with identification of oxidation products from OH-initiated reactions of TMBs and elucidation of the potential autoxidation pathway, Nitrate CI-API-TOF and Iodide CI-TOF were hence not calibrated and only the arbitrary signals with MS transmission correction (Heinritzi et al., 2016; Krechmer et al., 2018) were compared within the same instrument. It should then be noted that the relative signal intensities are biased among the MSs because of their ionization methods and transmission efficiency.

In each experiment, the Vocus PTR was used to confirm the establishment of stable precursor gas concentrations, and then the pair of 254 nm Hg lamps were turned on to generate the OH radicals and reaction products were analyzed by the MSs. The input RH in the OFR was kept at a low level and the voltage of the Hg lamps was slightly tuned in every experiment, so that the OH exposure in the OFR was

close to one oxidation lifetime of TMB (~~Kurylo and Orkin, 2003~~), i.e., consumption of ~~62.3%~~ $(1-1/e)$ of the initial TMB. Under this condition, the production of the first-generation products is generally ~~favoured~~favoured and the multi-generation products are also present, if the subsequent loss reactions for these products are assumed to proceed in the ~~same~~similar rate.

Table 1 summarizes all the experiments that were performed. Studied were 1,3,5-TMB ($\geq 99.0\%$, Aladdin), 1,2,3-TMB (Analytical standard, Aladdin), 1,2,4-TMB ($\geq 99.5\%$, Aladdin), 1,2,4-(1-methyl-D3)-TMB ($\geq 95\%$, Qingdao Tenglong Weibo Technology Co., Ltd., China), 1,2,4-(2-methyl-D3)-TMB ($\geq 95\%$, Qingdao Tenglong Weibo Technology Co., Ltd., China), and 1,2,4-(4-methyl-D3)-TMB ($\geq 95\%$, Qingdao Tenglong Weibo Technology Co., Ltd., China). The structure of these partially deuterated TMBs can be found in Figure S1. Note that ozone reactions were not taken into account in this study, because ozone reacts with aromatics at negligible rates, and its reaction rate with oxidation products containing C=C double bonds is much slower compared with that of OH (Jenkin et al., 1997, 2003; Molteni et al., 2018; Saunders et al., 2003). Also note that the concentrations of precursors in our experiments were much higher than the atmospheric ones. These concentrations were deliberately chosen to help identify the highly oxygenated products that are of low volatility and easy to loss in the sampling, but subject to the side effect that the relative significance of different pathways could be altered.

3 Results and discussion

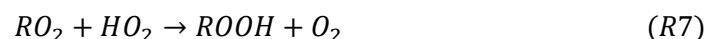
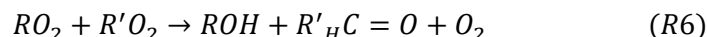
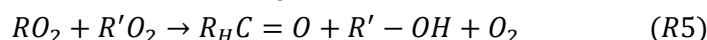
3.1 Characteristics of C9 products

Figure 2 presents an overview of C7, C8 and C9 products in a carbon oxidation state (\overline{OS}_C)-carbon number (n_C) space as observed by three MSs and also those predicted by MCM v3.3.1. Carbon oxidation state is a quantity that increases with the level of oxidation, which reveals the chemical aging of atmospheric organics (Kroll et al., 2011). It is evident that more species were detected by the three MSs, and although there were clear differences between products detected from different MSs, results indicate missing oxidation pathways in the current versions of the MCM (MCM v3.3.1, available at: <http://mcm.leeds.ac.uk/MCM>). Oxygen-containing C9 products were formed by adding functional groups to the carbon skeleton, whereas C7 and C8 products resulted from carbon-carbon scission of the original carbon skeleton together with functionalization. A large proportion of C7-C9 products were more oxidized than those predicted by MCM, hinting the existence of highly efficient oxidation pathways. ~~At the same time, some of the C7 and C8 products were characterized with unexpected low \overline{OS}_C , of which a few were even less oxidised than the precursor. The observation of these products is another indication for the existence of missing pathways in the current oxidation mechanisms.~~

Recent studies have emphasized on the importance of the peroxide-bicyclic pathway in producing highly oxygenated compounds in the oxidation of alkylbenzenes (Wang et al., 2017; Zaytsev et al., 2019), which leads to the formation of ring-retaining products. Therefore, here we further investigated C9 products of TMB oxidation detected by the three MSs (Figure 3). $C_9H_{10}O_{1-6}$, $C_9H_{12}O_{1-7}$, and $C_9H_{14}O_{4-6}$ contributed to the most of the signal intensities in Vocus PTR (Figure 3a). Compounds with fewer hydrogen atoms than TMB in Vocus PTR might be formed from hydrogen abstraction reactions. Iodide CI-TOF detected products with five to seven oxygen atoms (Figures 3b & 3c), which is narrower compared with Vocus PTR and Nitrate CI-APi-TOF. Molecules with 18 hydrogen atoms were detected only in Iodide CI-TOF, which

is an unexpected high number. These molecules, low in signal intensities in both gas and particle phases, might be formed from multiple OH attacks since each OH attack can only add two hydrogens in maximum onto the parent molecule. The species with the highest signal intensities measured in the gas phase appeared to be C₉H₁₂O₄, C₉H₁₂O₆, C₉H₁₄O₅, and C₉H₁₄O₆ in the 1,2,4-TMB + OH experiment, C₉H₁₄O₅ and C₉H₁₄O₆ in the 1,3,5-TMB + OH experiment, and C₉H₁₂O₆ and C₉H₁₂O₇ in the 1,2,3-TMB + OH experiment (Figure 3b). Compared with the gas phase, more oxidized particulate products tended to contribute a larger proportion of signal in FIGAERO-Iodide-CI-APi-TOF (Figure 3c). Nevertheless, the gas phase products are emphasized in the current study, which can be detected by and compared among the three instruments. Nitrate CI-APi-TOF detected C₉ products containing 12-16 hydrogen atoms and 5-11 oxygen atoms (Figure 3d).

RO₂ radicals can react in the absence of NO, to form termination products including carbonyls, alcohols, and hydroperoxides via the following reactions (Mentel et al., 2015).



Here we present a criteria method based on the work of Mentel et al. (2015). For a parent peroxy radical with a molecular mass of m , its termination ought to lead to the formation of a carbonyl, an alcohol, and a hydroperoxyl, which have a molecular mass of $m-17$, $m-15$, and $m+1$, respectively. Since elemental formulas as determined by the high-resolution MS do not contain information regarding functional groups or the structure of a molecule, the identified mass spectral signals could be counted as either one of the three categories. Listed in Table 2 are detected stabilized oxidation products in categories of carbonyl, alcohol, and hydroperoxyl, which hints the potential existence of the corresponding peroxy radicals. These stabilized products all contain six or more oxygen atoms, which meet the definition of HOMs (Bianchi et al., 2019). C₉H₁₂O₆ is one of the only two signals that have been predicted by MCM~~the only signal that has been predicted by MCM~~, assumed to be a hydroperoxyl product from a ring-opening peroxy radical that goes through multiple OH attack reactions (MCM name: C7MOCOCO3H), which is unlikely to contribute a lot to the observed signal of C₉H₁₂O₆ since the concentration of a multi-generation product is not expected to be high at OH exposure as short as one lifetime of TMB~~which is unlikely to occur under our experimental conditions~~. C₉H₁₄O₆ is the other one, presumed to be a hydroperoxyl product of a second-generation peroxy radical formed via epoxy-oxy pathway (MCM name: TM124MUOOH), which is unlikely to be formed through the MCM route with a considerable yield, either. Four pairs of peroxy radicals, i.e., C₉H₁₃O₇[•] and C₉H₁₃O₉[•], C₉H₁₃O₈[•] and C₉H₁₃O₁₀[•], C₉H₁₅O₇[•] and C₉H₁₅O₉[•], and C₉H₁₅O₈[•] and C₉H₁₅O₁₀[•], can be selected from the eight potential peroxy radicals in Table 2. The molecular formulas for the peroxy radicals within each pair differ by 2 × O, which is a first evidence for the autoxidation pathway.

3.2 Autoxidation mechanisms of 1,2,4-TMB

The autoxidation pathways were then further elucidated by experiments with isotopically labelled precursors, 1,2,4-(1-methyl-D3)-TMB, 1,2,4-(2-methyl-D3)-TMB, and 1,2,4-(4-methyl-D3)-TMB, whose structure is shown in Figure S1.

If an intramolecular hydrogen shift happens during autoxidation with the abstracted hydrogen coming from a methyl group, molecular oxygen will rapidly attach to this carbon-centred radical to form a new alkyl peroxy radical (Bianchi et al., 2019 and reference herein). One potential fate of this R-CH₂OO• radical is to lose one of the two remaining hydrogen atoms, forming a carbonyl according to Reaction R5. Thus, one of the three original hydrogen atoms in the methyl group will leave this molecule after an autoxidation step (Ehn et al., 2014; Mentel et al., 2015; Molteni et al., 2018; Otkjær et al., 2018; Rissanen et al., 2014; Wang et al., 2017). In the case of a deuterium abstraction from a methyl-D3 group during the autoxidation, an oxidation product with two deuterium atoms (C₉H₇D₂O_z) will then be formed, which is presumably a carbonyl. Although an alcohol or a hydroperoxyl could also be formed from a peroxy radical, it is not suitable to utilize the presence of alcohol and hydroperoxyl products as a criteria to judge the existence of autoxidation. The hydroxyl channel of deuterated peroxy radicals can lead to the formation of alcohol products with either 3 or 4 deuterium atoms, depending on the nature of the other reacting RO₂. The slow unimolecular reaction rate of deuterated methyl group corresponds to little formation of the products with 4 deuterium atoms, whereas our MSs cannot differentiate 3 deuterium atoms either from a molecule with autoxidation and hydroxyl termination or from an untouched methyl-D3 group. On the other hand, the hydroperoxyl channel would lead to the formation of hydroperoxyl products with 3 deuterium atoms, too. Therefore, only the carbonyl channel products of a peroxy radical was used to suggest the potential autoxidation that has occurred.

Table 3 ~~summaries~~ summarizes two-deuterium-containing C9 (C₉H₇D₂O_z) products that were detected by Vocus PTR and Nitrate CI-API-TOF in different isotope labelling experiments: C₉H₁₀D₂O₆ in the 1,2,4-(1-methyl-D3)-TMB + OH experiment by Vocus PTR and Nitrate CI-API-TOF; C₉H₁₀D₂O₇ in the 1,2,4-(1-methyl-D3)-TMB + OH experiment by Vocus PTR; and C₉H₁₂D₂O₈ in the 1,2,4-(4-methyl-D3)-TMB + OH experiment by Nitrate CI-API-TOF. C₉H₁₀O₇D₂ (234.0703 Th) was expected to be detected by Nitrate CI-API-TOF, but unfortunately an undefined peak (located at 295.9827 Th) covered the position where C₉H₁₀O₇D₂•NO₃⁻ (296.0592 Th) was supposed to been identified. C₉H₁₂D₂O₈ (252.0814 Th) was not detected by Vocus PTR, likely owing to either its low proton affinity or its partitioning onto the inlet of Vocus PTR, given its high O:C ratio and hence low volatility. However, Nitrate CI-API-TOF was able to detect this very sticky compound, because the nitrate source is constructed with concentric sample and sheath flows that minimize the diffusive losses of samples to the source wall. These results indicate that an intramolecular deuterium-migration happened on the 1-methyl-D3 substituent of the C₉H₁₀D₃O₄ and C₉H₁₀D₃O₅ radicals, and the 4-methyl-D3 substituent of the C₉H₁₂D₃O₇ radical, respectively, then one oxygen was added to the resulting alkyl radicals, and the new peroxy radical reacted to form C₉H₁₀D₂O₆, C₉H₁₀D₂O₇, and C₉H₁₂D₂O₉, respectively.

These three compounds (C₉H₁₀D₂O₆, C₉H₁₀D₂O₇, and C₉H₁₂D₂O₉) did not possess high signal intensities, because the deuterium transfer reactions are typically significantly slower for D (²H) nuclei than hydrogen transfer reactions for H (¹H) (Bianchi et al., 2019; Wang et al., 2017). There might be other two-deuterium-containing C9 products in these experiments. However, since many of these signals were at the instrument detection limits or even lower, the nonideal experimental conditions prevent us from confirming more such compounds.

Based on the observed signals of two-deuterium-containing C9 products and structures that have been previously proven to favor H-shift reactions (Otkjær et al., 2018), two plausible formation pathways for the observed products are proposed.

The first one starts with a BPR of $C_9H_{13}O_5^\bullet$ as shown in Scheme 1, which is the first BPR formed from C_9H_{12} via the peroxide-bicyclic pathway. The structure of this particular $C_9H_{13}O_5^\bullet$ is different from what is proposed in MCM v3.3.1, but the position for the initial OH attack, i.e., the 4th carbon on the ring, is feasible owing to the attraction of a substituted group on its para-position (Li and Wang, 2014), and the subsequent addition of O_2 after the initial OH attack along with bicyclization occurs on the same relative position as previous studies have suggested (Bloss et al., 2005; Jenkin et al., 2003). The resulting BPR of $C_9H_{13}O_5^\bullet$ undergoes a hydrogen shift, during which the abstracted hydrogen comes from the methyl terminal of an allylic group. This hydrogen is much easier to be abstracted, compared to those in a normal methyl group that are unlikely to go through a hydrogen shift with a peroxy radical (Otkjær et al., 2018). The new BPR of $C_9H_{13}O_7^\bullet$ then reacts via R5, R6, and R7 to form $C_9H_{12}O_6$, $C_9H_{14}O_6$, and $C_9H_{14}O_7$, respectively. This pathway is suggested by the observation of $C_9H_{10}D_2O_6$ in the 1,2,4-(1-methyl-D3)-TMB + OH experiment. ~~On the other hand, $C_9H_{13}O_5^\bullet$ can alternatively self-react or react with a HO_2 radical to form an alkoxy intermediate, which goes through isomerization and addition of an oxygen to form a BPR of $C_9H_{13}O_8^\bullet$. The stabilized products from $C_9H_{13}O_8^\bullet$ include $C_9H_{12}O_7$, $C_9H_{14}O_7$, and $C_9H_{14}O_8$. This pathway is suggested by the observation of $C_9H_{10}D_2O_7$ in the 1,2,4-(1-methyl-D3)-TMB + OH experiment.~~

It's noted that in all the three isotope experiments, we also detected products of $C_9H_9D_3O_6$ and $C_9H_9D_3O_7$ with much higher signal intensities, indicating the existence of other autooxidation pathways. Thus, it deserves a repeated emphasis here that we only point out feasible pathways that are supported by our isotope experiments in this work, but do not rule out other possibilities.

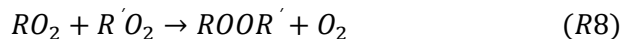
The second pathway is described in scheme 2. This pathway starts from a BPR of $C_9H_{13}O_5^\bullet$ that is formed by the initial OH attack and subsequent reactions. MCM v3.3.1 includes a BPR with the same structure but does not contain the subsequent reactions. The BPR of $C_9H_{13}O_5^\bullet$ can be terminated via R5, forming a stabilized hydroxyl product of $C_9H_{14}O_4$, which is subject to a second OH attack and a following addition of O_2 , resulting in a new peroxy radical of $C_9H_{15}O_7^\bullet$. There are no systematic investigations on the effect of a peroxide-bicyclic substitution on the 1,5 H-shift rate constant. However, our data indicate a hydrogen shift can occur on the 4-methyl group, based on which the structure of $C_9H_{15}O_9^\bullet$ is proposed. The new BPR of $C_9H_{15}O_9^\bullet$ is then terminated via R5, R6, and R7, forming stabilized products $C_9H_{14}O_8$, $C_9H_{16}O_8$, and $C_9H_{16}O_9$, respectively. This pathway is suggested by the observation of $C_9H_{12}D_2O_8$ in the 1,2,4-(4-methyl-D3)-TMB + OH experiment, though other pathways could result in products with the same formula.

An autooxidation reaction pathway that can explain the observation of $C_9H_{10}D_2O_7$ in the 1,2,4-(1-methyl-D3)-TMB + OH experiment is currently unavailable, although we speculate that a “peroxy-alkoxy-peroxy” conversion is likely involved during the formation of $C_9H_{12}O_7$ according to the number of oxygen atoms.

3.3 Characteristics of C18 HOMs

Products with 18 carbon atoms were observed in our experiments by Nitrate CI-API-TOF, all containing 24-30 hydrogen atoms and 8 or more oxygen atoms ($C_{18}H_{24/26/28/30}O_{>8}$) (Figure 4). C18 products with 26 or 28 hydrogen atoms contributed the most of the signal intensities while those generated by 1,3,5-

TMB were the most abundant. Recent studies revealed that long-neglected organic peroxide dimer (ROOR') formation reactions might be an important source of gas-phase dimer compounds, through which two peroxy radicals form accretion products consisting of the carbon backbone of both reactants (Berndt et al., 2018a, 2018b; Zhao et al., 2018).



This reaction has been proved to be another important loss process for RO₂ radicals formed via autoxidation. On account of their extraordinarily low vapor pressure, HOM dimers contribute more significantly to the formation and growth of atmospheric new particles than HOM monomers.

Our C18 oxidation products have similar ion formulas to the dimer products in recent 1,3,5-TMB oxidation experiments (Molteni et al, 2018; Tsiligiannis et al., 2019). In our experiments, the formation of C₁₈H₂₆O₈₋₁₅, C₁₈H₂₈O₉₋₁₅, and C₁₈H₃₀O₁₂₋₁₅ can be explained by reactions of two C₉H₁₃O_x•, one C₉H₁₃O_x• and one C₉H₁₅O_x•, and two C₉H₁₅O_x• respectively. C₁₈H₂₄O₈₋₁₃ with low signal intensities were detected by Nitrate CI-API-TOF, hinting that H-abstraction reactions have occurred leading to a lower hydrogen atom in the product than in the precursor.

Figure 5 summarizes the relative contribution of C9 and C18 products formed from TMB oxidation as detected by Nitrate CI-API-TOF. The charge-charging efficiency for C9 and C18 products is assumed to be identical in Nitrate CI-API-TOF (Ehn et al., 2014; Hyttinen et al., 2015). Hence, the measured relative abundances of the oxidation products, with corrections of the transmission function in the MS, can faithfully represent the product distribution in the experiments. In the Exp. #1-3, the dimers (C₁₈H₂₆O₈₋₁₅) formed from two C₉H₁₃O_x• along those (C₁₈H₂₈O₉₋₁₅) from one C₉H₁₃O_x• and one C₉H₁₅O_x• contributed the most intensity, whereas the most intensive C9 products (C₉H₁₄O₅₋₁₁) could be the alcohol or hydroperoxyl products of C₉H₁₃O_x•, or the carbonyl products of C₉H₁₅O_x• (Table S1). 1,2,3-TMB produced the most C9 products, 1,2,4-TMB the second, and 1,3,5-TMB the least. An opposite trend was observed for C18 products. Therefore, the reduction of C9 products was likely due to the dimer formation. Here, we define the C18 fraction as the ratio of the signal intensities of C18 products to the sum of those of C9 and C18 products in Nitrate CI-API-TOF, and the C9 fraction in a similar way. According to our results, the dimer fraction was the highest for aromatics with meta-substituents and the least for aromatics with ortho-substituents, if the number and size of substituted groups are identical, while the monomer fraction had an opposite tendency. This can be explained by the stereoselectivity of accretion formation reactions.

In the 1,3,5-TMB oxidation experiments (Exp. #2), where the highest C18 dimer fraction was observed, the mole fraction of the C18 dimers is likely determined by the competition of reactions R5, R6, R7, and R8, which can be mathematically expressed as

$$f_{C18} = \frac{0.5 \times k_{R8}[RO_2]}{k_{R5,R6}[RO_2] + k_{R7}[HO_2] + 0.5 \times k_{R8}[RO_2]} \quad (1)$$

where $k_{R5,R6}$ stands for the reaction rates for R5 and R6, assumed to be around $8.8 \times 10^{-13} \text{ cm}^3 \text{ molecule}^{-1} \text{ s}^{-1}$ by MCM, k_{R7} is the reaction rate for R7, set at a typical value of $2 \times 10^{-11} \text{ cm}^3 \text{ molecule}^{-1} \text{ s}^{-1}$ (Berndt et al., 2018b; Bianchi et al., 2019), and k_{R8} is the reaction rate of R8 for BPRs generated by 1,3,5-TMB, which has recently been measured to be as fast as $10^{-10} \text{ cm}^3 \text{ molecule}^{-1} \text{ s}^{-1}$ (Berndt et al., 2018b).

Since the concentration of HO₂ in the OFR was not measured, we utilized a kinetic reaction model (PAM_chem_v8) to characterize the concentration profiles of oxidants in the OFR, which include OH, O₃,

HO₂, and H₂O₂. A detailed description of this model is given in Section S1 of the supplement and the modelled profiles of oxidants and precursors are shown in Figure S4. According to the model, the steady-state concentration of HO₂ in the Exp. #2 was around 18 ppt ($\sim 4.5 \times 10^8$ molecules cm⁻³). On the other hand, it is difficult to evaluate the effective concentration of the RO₂ radicals in the system, because RO₂ with low oxidation states will not form HOMs via reactions R5-R8. Therefore, we estimated the concentration of RO₂ in Eq. (1) to be close to that of BPRs in the OFR. According to MCM v3.3.1, the branching ratio for the peroxide-bicyclic pathway in the OH oxidation of 1,3,5-TMB is 79%, so that the concentration of BPRs was roughly estimated to be 58.5 ppb ($\sim 1.5 \times 10^{12}$ molecules cm⁻³, 79% of the reacted 1,3,5-TMB). Hence, the fraction of C18 dimer is estimated to be around 98%. Clearly, this estimation itself comes with a large uncertainty, and the estimated fraction can only be regarded as an indication of explainable high yields of C18 dimers instead of a rigorous number.

In fact, under our experimental conditions, ~~Under our experimental conditions,~~ the C18 dimer fraction in the 1,3,5-TMB experiments was around 86.5%, which is much higher than the dimer fraction of 42.6%-56.5% re-calculated using the measured C9 and C18 signals by Tsiligiannis et al. (2019), 43.3%-52.4% modelled by Tsiligiannis et al. (2019), and 39% reported by Molteni et al. (2018). The lack of a m/z-transmission correction in the former two studies could partially explain the discrepancy (Molteni et al., 2018; Tsiligiannis et al., 2019). On the other hand, this observation could also be due to the much higher RO₂ concentrations in our experiments. The amount of reacted 1,3,5-TMB in our experiment is around 74.1 ppb ($\sim 1.8 \times 10^{12}$ molecules cm⁻³), whereas in the experiments of Tsiligiannis et al. (2019) and Molteni et al. (2018), the numbers are 26 ppb ($\sim 6.5 \times 10^{11}$ molecules cm⁻³) and 22.3 ppb ($\sim 5.6 \times 10^{11}$ molecules cm⁻³), respectively. Again, it should be reminded that this result was obtained under the condition of very high concentrations of precursors and thus the relative fractions of products could be different under the ambient conditions.

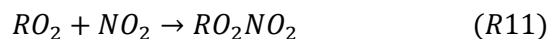
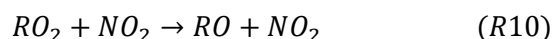
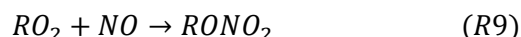
3.4 Influence of NO_x

To constrain the NO_x level in the OFR, the profiles of NO/NO₂ were modelled by PAM_chem_v8, as shown in Figure S5. The mathematically-averaged NO_x levels in the low NO_x experiment (Exp. #7) and higher NO_x experiment (Exp. #8) were 92 ppb (2.5 ppb NO + 89.5 ppb NO₂) and 295.3 ppb (2.9 ppb NO + 292.4 ppb NO₂), respectively. The NO_x/VOC in our experiments is comparable to ambient values in polluted areas. The NO_x/(ΔVOC) was around 0.9 in the low NO_x experiment and 2.9 in the higher NO_x one.

Figure 6 describes the distribution of C9 products detected by Nitrate CI-APi-TOF in the absence of NO_x (Exp. #1), a low NO_x experiment (Exp. #7), and a higher NO_x experiment (Exp. #8), respectively. Once NO_x was added, the formation of C9 non-nitrogen products declined down to around 20% of those in Exp. #1. The production of C9 non-nitrogen products did not decrease much between low NO_x experiment and higher NO_x experiment, indicating a nonlinear effect of NO_x on the production of C9 non-nitrogen products. Dinitrates (C₉H_xN₂O_y) increased with the NO_x concentration, but C9 organonitrates (ONs, C₉H_xNO_y) slightly reduced in the higher NO_x experiment compared to that in the low one, which indicates a complex competition between RO₂ + RO₂ and RO₂ + NO_x.

The observation of C9 products containing 1-2 nitrogen atoms and C18 products with one nitrogen atom is similar to the results for 1,3,5-TMB oxidation experiments in the presence of NO_x reported by

Tsiligiannis et al. (2019). NO_x can perturb the fate of peroxy radicals by the following reactions (Orlando and Tyndall, 2012; Rissanen, 2018):



Competing with the other RO₂ reactions, NO_x can dramatically reduce the formation of C9 non-nitrogen products. ~~The NO_x levels in the low NO_x experiment (Exp. #7) and higher NO_x experiment (Exp. #8) were 0.8 ppb and 6.5 ppb, respectively. Compared to the ambient values in polluted areas, this NO_x/VOC is low. The NO_x/(ΔVOC) was around 0.8% in the low NO_x experiment and 6.4% in higher NO_x one.~~

Most organonitrates observed in our study were characterized with 13 hydrogen atoms, as detected by Nitrate CI-API-TOF (Figure S2). All of them contained more than 6 oxygen atoms, with molecular formulas corresponding to bicyclic organonitrates formed from termination reactions of C₉H₁₃O_x• with NO or NO₂ (i.e., pathway R9 and R11, respectively). The dinitrates were dominated by species with 14 hydrogen atoms (Figure S3). As suggested by Tsiligiannis et al. (2019), an OH radical could attack a nitrated compound that is formed from NO_x termination of a peroxy radical, then an oxygen atom is added (similarly to the reactions from C₉H₁₄O₇ to C₉H₁₅O₇ in scheme 2), and then the newly formed peroxy radical that have already contained one nitrogen will be terminated by NO or NO₂ again. Therefore, most of the detected dinitrates were also formed from C₉H₁₃O_x•.

Figure 7a describes the relative intensities of C18 HOMs in Exp. #7, and Exp. #8 as detected by Nitrate CI-API-TOF, in comparison with their relative intensities in Exp. #1. The relative intensities of most of the C18 HOMs decreased with the NO_x/(ΔVOC), while a few of the C18 HOMs including C₁₈H₂₄O₁₃, C₁₈H₂₆O₁₃, C₁₈H₂₆O₁₄, C₁₈H₂₈O₁₂ increased slightly in the higher NO_x experiment, potentially from a combined effect of NO_x and OH. The injection of NO_x can compete with the other RO₂ reactions, and thus it consumes peroxy radicals that would otherwise go through accretion reactions, which explains the decrease of most C18 HOMs. On the other hand, the introduction of NO_x can increase the oxidation capacity in the OFR, as it does in the ambient environment, leading to the slight enhancement for the few C18 HOMs. After the addition of NO_x, all of the C18 HOMs decreased by more than six times compared with those in no NO_x experiments, indicating that the dimers were more strongly influenced than monomers, which is in agreement with a previous study (Tsiligiannis et al., 2019).

The C18 ONs with 25 or 27 hydrogen atoms were detected in the NO_x experiments (Figure 7b). Other C18 products containing nitrogen atoms were not detected. The C₁₈H₂₅NO_x might be formed from reactions between a C₉H₁₂NO_x• radical and a C₉H₁₃O_x• radical, or between a C₉H₁₄NO_x• and a C₉H₁₁O_x• radical, all of which existed in the system. The C₁₈H₂₇NO_x is most likely to be formed from reactions between a C₉H₁₄NO_x• radical and a C₉H₁₃O_x• radical, which were the most abundant C9 radicals. All the C18 ONs decreased with the increase of NO_x/(ΔVOC), which is reasonable. Introduction of NO_x into the system triggered reactions between C9 peroxy radicals and NO_x, which consequently reduced the formation of accretion products like C18 ONs.

4 Conclusions

The identities and distribution of oxidation products formed from OH-initiated reactions of three TMBs were obtained with a suite of state-of-the-art chemical ionization mass spectrometers. Our recent study shows that the ring-retaining products are more oxygenated and quite a lot of carbon-carbon scission products are missed in the current model, indicating that the degradation products of aromatics are much more diverse than what is available in MCM (Mehra et al., 2020). Because of its important contribution to the nucleation and SOA formation in urban areas, the ring-retaining products of TMB deserve a more detailed characterization. Here we have built on that work by showing the formation pathways of ring-retaining highly oxygenated products and through identification of accretion products.

With the assistance of three 1,2,4-(methyl-D3)-TMB experiments we have demonstrated that the rapid formation of HOMs is attributable to the autoxidation pathway during the TMB oxidation. Several plausible autoxidation pathways for OH-initiated reactions of 1,2,4-TMB were proposed, emphasizing on the ring-retaining pathways of aromatics, especially the bicyclic-peroxide channel, which is followed by autoxidation that is not shown in the current models, such as MCM. Oxidation of aromatic VOCs was shown in our study to produce HOM dimers, which might be underestimated or even completely ignored in previous studies which utilize techniques not capable of detecting dimers. The structural enhancement for accretion product formation via the $\text{RO}_2 + \text{R}'\text{O}_2$ reaction has been observed, of which the meta-substituents was shown to be strongest and ortho-substituents the weakest, though the detailed stereoselectivity for aromatics remains unclear now.

In the presence of NO_x whose reaction with $\text{RO}_2\cdot$ can compete with $\text{RO}_2\cdot + \text{RO}_2\cdot$ or $\text{RO}_2\cdot + \text{HO}_2\cdot$ reactions, ONs and dinitrates will be generated via reactions of NO_x with BPRs in 1,2,4-TMB oxidation system, and dimer products with one nitrogen will be formed via the subsequent reactions. This is consistent with a recent ambient observations in the polluted environment, where ONs, dinitrates, and nitrogen-containing dimers presumably formed from BVOCs and alkylbenzenes were detected (Brean et al., 2019). The formation of ONs and dinitrates from TMB is not linearly ~~depending~~ dependent on the NO_x concentration, which excludes the possibility of extrapolating our laboratory results to ambient conditions. Nevertheless, the changes of HOM compositions in the presence of NO_x , especially the accretion products, could have an effect on NPF and SOA formation. Previous work has showed that the ring-retaining product formation at NO_x environment tends to be more important for TMB than other single substituted C9 aromatics, i.e., isopropylbenzene and propylbenzene, which emphasized the significance of TMB ring-retaining oxidation in the urban environment (Mehra et al., 2020). Further research is needed to acquire a quantitative understanding of the role of NO_x in HOM formation.

Clearly, these multifunctional gas phase products appear at different stages of the oxidation chain. These mass spectra can be used as ideal “fingerprints” of TMB oxidation in the ambient gas phase measurement to elucidate atmospheric oxidation conditions.

Data availability. Data related to this article will be available from a persistent repository and upon request from corresponding authors.

Supplement. The supplement related to this article is available online.

522 *Author contributions.* LW, and YW designed the experiments. YW, GY, XH, and YL carried out the
523 instrument deployment and operation. AM, JK, and AL provided technical support. YW analyzed the data.
524 YW, LW, and JK wrote the paper. All co-authors discussed the results and commented on the manuscript.
525
526 *Competing interests.* The authors declare that they have no conflict of interest.
527
528 *Acknowledgments.* This work was financially supported by the National Natural Science Foundation of
529 China (91644213, 21925601) and the National Key R&D Program of China (2017YFC0209505). Lin
530 Wang acknowledges the Newton Advanced Fellowship (NA140106).

References

- Atkinson, R.: Kinetics and Mechanisms of the Gas-Phase Reactions of the Hydroxyl Radical with Organic Compounds under Atmospheric Conditions, *Chem. Rev.*, 86(1), 69–201, doi:10.1021/cr00071a004, 1986.
- Atkinson, R. and Arey, J.: Atmospheric Degradation of Volatile Organic Compounds, *Chem. Rev.*, 103(12), 4605–4638, doi:10.1021/cr0206420, 2003.
- Atkinson, R. and Carter, W. P. L.: Kinetics and Mechanisms of the Gas-Phase Reactions of Ozone with Organic Compounds under Atmospheric Conditions, *Chem. Rev.*, 84(5), 437–470, doi:10.1021/cr00063a002, 1984.
- Berndt, T., Richters, S., Jokinen, T., Hyttinen, N., Kurtén, T., Otkjær, R. V., Kjaergaard, H. G., Stratmann, F., Herrmann, H., Sipilä, M., Kulmala, M. and Ehn, M.: Hydroxyl radical-induced formation of highly oxidized organic compounds, *Nat. Commun.*, 7(May), doi:10.1038/ncomms13677, 2016.
- Berndt, T., Mentler, B., Scholz, W., Fischer, L., Herrmann, H., Kulmala, M. and Hansel, A.: Accretion Product Formation from Ozonolysis and OH Radical Reaction of α -Pinene: Mechanistic Insight and the Influence of Isoprene and Ethylene, *Environ. Sci. Technol.*, 52(19), 11069–11077, doi:10.1021/acs.est.8b02210, 2018a.
- Berndt, T., Scholz, W., Mentler, B., Fischer, L., Herrmann, H., Kulmala, M. and Hansel, A.: Accretion Product Formation from Self- and Cross-Reactions of RO₂ Radicals in the Atmosphere, *Angew. Chemie Int. Ed.*, 57(14), 3820–3824, doi:10.1002/anie.201710989, 2018b.
- Berndt, T., Scholz, W., Mentler, B., Fischer, L., Herrmann, H., Kulmala, M. and Hansel, A.: Accretion Product Formation from Self- and Cross-Reactions of RO₂ Radicals in the Atmosphere, *Angew. Chemie Int. Ed.*, 57(14), 3820–3824, doi:10.1002/anie.201710989, 2018c.
- Bianchi, F., Kurtén, T., Riva, M., Mohr, C., Rissanen, M. P., Roldin, P., Berndt, T., Crounse, J. D., Wennberg, P. O., Mentel, T. F., Wildt, J., Junninen, H., Jokinen, T., Kulmala, M., Worsnop, D. R., Thornton, J. A., Donahue, N., Kjaergaard, H. G. and Ehn, M.: Highly Oxygenated Organic Molecules (HOM) from Gas-Phase Autoxidation Involving Peroxy Radicals: A Key Contributor to Atmospheric Aerosol, *Chem. Rev.*, 119(6), 3472–3509, doi:10.1021/acs.chemrev.8b00395, 2019.
- Bloss, C., Wagner, V., Jenkin, M. E., Volkamer, R., Bloss, W. J., Lee, J. D., Heard, D. E., Wirtz, K., Martin-Reviejo, M., Rea, G., Wenger, J. C. and Pilling, M. J.: Development of a detailed chemical mechanism (MCMv3.1) for the atmospheric oxidation of aromatic hydrocarbons, *Atmos. Chem. Phys.*, 5(3), 641–664, doi:10.5194/acp-5-641-2005, 2005a.
- Bloss, C., Wagner, V., Bonzanini, A., Jenkin, M. E., Wirtz, K., Martin-Reviejo, M. and Pilling, M. J.: Evaluation of detailed aromatic mechanisms (MCMv3 and MCMv3.1) against environmental chamber data., 2005b.
- Brean, J., Harrison, R. M., Shi, Z., Beddows, D. C. S., Acton, W. J. F., Nicholas Hewitt, C., Squires, F. A. and Lee, J.: Observations of highly oxidized molecules and particle nucleation in the atmosphere of Beijing, *Atmos. Chem. Phys.*, doi:10.5194/acp-19-14933-2019, 2019.
- Calvert, J. G., Atkinson, R., Kerr, J. a., Madronich, S., Moortgat, G. K., Wallington, T. J. and Yarwood, G.: *The Mechanisms of Atmospheric Oxidation of the Alkenes.*, 2000.
- Crounse, J. D., Nielsen, L. B., Jørgensen, S., Kjaergaard, H. G. and Wennberg, P. O.: Autoxidation of organic compounds in the atmosphere, *J. Phys. Chem. Lett.*, 4(20), 3513–3520, doi:10.1021/jz4019207, 2013.
- D'Ambro, E. L., Lee, B. H., Liu, J., Shilling, J. E., Gaston, C. J., Lopez-Hilfiker, F. D., Schobesberger, S., Zaveri, R. A., Mohr, C., Lutz, A., Zhang, Z., Gold, A., Surratt, J. D., Rivera-Rios, J. C., Keutsch, F. N. and Thornton, J. A.: Molecular composition and volatility of isoprene photochemical oxidation secondary organic aerosol under low- and high-NO_x conditions, *Atmos. Chem. Phys.*, 17(1), 159–174, doi:10.5194/acp-17-159-2017, 2017.
- Ehn, M., Thornton, J. A., Kleist, E., Sipilä, M., Junninen, H., Pullinen, I., Springer, M., Rubach, F., Tillmann, R., Lee, B., Lopez-Hilfiker, F., Andres, S., Acir, I. H., Rissanen, M., Jokinen, T., Schobesberger, S., Kangasluoma, J., Kontkanen, J., Nieminen, T., Kurtén, T., Nielsen, L. B., Jørgensen, S., Kjaergaard, H. G., Canagaratna, M., Maso, M. D., Berndt, T., Petäjä, T., Wahner, A., Kerminen, V. M., Kulmala, M., Worsnop, D. R., Wildt, J. and Mentel, T. F.: A large source of low-volatility secondary organic aerosol, *Nature*, 506(7489), 476–479, doi:10.1038/nature13032, 2014.
- Eisele, F. L. and Tanner, D. J.: Measurement of the gas phase concentration of H₂SO₄ and methane sulfonic acid and estimates of H₂SO₄ production and loss in the atmosphere, *J. Geophys. Res.*, doi:10.1029/93JD00031, 1993.
- Garmash, O., Rissanen, M. P., Pullinen, I., Schmitt, S., Kausiala, O., Tillmann, R., Percival, C., Bannan, T. J., Priestley, M., Hallquist, Å. M., Kleist, E., Kiendler-Scharr, A., Hallquist, M., Berndt, T., McFiggans, G., Wildt, J., Mentel, T., Ehn, M. and Garmash olgagarmash, O.: Multi-generation OH oxidation as a source for highly oxygenated organic molecules from aromatics, *Atmos. Chem. Phys. Discuss*, doi:10.5194/acp-2019-582, 2019.
- Gueneron, M., Erickson, M. H., Vanderschelden, G. S. and Jobson, B. T.: PTR-MS fragmentation patterns of

- gasoline hydrocarbons, *Int. J. Mass Spectrom.*, 379, 97–109, doi:10.1016/j.ijms.2015.01.001, 2015.
- Hallquist, M., Wenger, J. C., Baltensperger, U., Rudich, Y., Simpson, D., Claeys, M., Dommen, J., Donahue, N. M., George, C., Goldstein, A. H., Hamilton, J. F., Herrmann, H., Hoffmann, T., Iinuma, Y., Jang, M., Jenkin, M. E., Jimenez, J. L., Kiendler-Scharr, A., Maenhaut, W., McFiggans, G., Mentel, T. F., Monod, A., Prévôt, A. S. H., Seinfeld, J. H., Surratt, J. D., Szmigielski, R. and Wildt, J.: The formation, properties and impact of secondary organic aerosol: Current and emerging issues, *Atmos. Chem. Phys.*, 9(14), 5155–5236, doi:10.5194/acp-9-5155-2009, 2009.
- Heinritzi, M., Simon, M., Steiner, G., Wagner, A. C., Kürten, A., Hansel, A. and Curtius, J.: Characterization of the mass-dependent transmission efficiency of a CIMS, *Atmos. Meas. Tech.*, 9(4), 1449–1460, doi:10.5194/amt-9-1449-2016, 2016.
- Hyttinen, N., Kupiainen-Määttä, O., Rissanen, M. P., Muuronen, M., Ehn, M. and Kurtén, T.: Modeling the Charging of Highly Oxidized Cyclohexene Ozonolysis Products Using Nitrate-Based Chemical Ionization, *J. Phys. Chem. A*, 119(24), 6339–6345, doi:10.1021/acs.jpca.5b01818, 2015.
- Isaacman-VanWertz, G., Massoli, P., O'Brien, R. E., Nowak, J. B., Canagaratna, M. R., Jayne, J. T., Worsnop, D. R., Su, L., Knopf, D. A., Misztal, P. K., Arata, C., Goldstein, A. H. and Kroll, J. H.: Using advanced mass spectrometry techniques to fully characterize atmospheric organic carbon: current capabilities and remaining gaps, *Faraday Discuss.*, 200, 579–598, doi:10.1039/C7FD00021A, 2017.
- Jenkin, M. E., Saunders, S. M. and Pilling, M. J.: The tropospheric degradation of volatile organic compounds: A protocol for mechanism development, *Atmos. Environ.*, 31(1), 81–104, doi:10.1016/S1352-2310(96)00105-7, 1997.
- Jenkin, M. E., Saunders, S. M., Wagner, V. and Pilling, M. J.: Protocol for the development of the Master Chemical Mechanism, MCM v3 (Part B): tropospheric degradation of aromatic volatile organic compounds, *Atmos. Chem. Phys.*, 3(1), 181–193, doi:10.5194/acp-3-181-2003, 2003a.
- Jenkin, M. E., Saunders, S. M., Wagner, V. and Pilling, M. J.: Protocol for the development of the Master Chemical Mechanism, MCM v3 (Part B): tropospheric degradation of aromatic volatile organic compounds, *Atmos. Chem. Phys.*, 3(1), 181–193, doi:10.5194/acp-3-181-2003, 2003b.
- Jokinen, T., Sipilä, M., Richters, S., Kerminen, V. M., Paasonen, P., Stratmann, F., Worsnop, D., Kulmala, M., Ehn, M., Herrmann, H. and Berndt, T.: Rapid autoxidation forms highly oxidized RO₂ radicals in the atmosphere, *Angew. Chemie - Int. Ed.*, 53(52), 14596–14600, doi:10.1002/anie.201408566, 2014.
- Jokinen, T., Berndt, T., Makkonen, R., Kerminen, V. M., Junninen, H., Paasonen, P., Stratmann, F., Herrmann, H., Guenther, A. B., Worsnop, D. R., Kulmala, M., Ehn, M. and Sipilä, M.: Production of extremely low volatile organic compounds from biogenic emissions: Measured yields and atmospheric implications, *Proc. Natl. Acad. Sci. U. S. A.*, 112(23), 7123–7128, doi:10.1073/pnas.1423977112, 2015.
- Jørgensen, S., Knap, H. C., Otkjær, R. V., Jensen, A. M., Kjeldsen, M. L. H., Wennberg, P. O. and Kjaergaard, H. G.: Rapid Hydrogen Shift Scrambling in Hydroperoxy-Substituted Organic Peroxy Radicals, *J. Phys. Chem. A*, 120(2), 266–275, doi:10.1021/acs.jpca.5b06768, 2016.
- Krechmer, J., Lopez-Hilfiker, F., Koss, A., Hutterli, M., Stoermer, C., Deming, B., Kimmel, J., Warneke, C., Holzinger, R., Jayne, J., Worsnop, D., Fuhrer, K., Gonin, M. and De Gouw, J.: Evaluation of a New Reagent-Ion Source and Focusing Ion–Molecule Reactor for Use in Proton-Transfer-Reaction Mass Spectrometry, *Anal. Chem.*, 90, 12011–12018, doi:10.1021/acs.analchem.8b02641, 2018.
- Krechmer, J. E., Coggon, M. M., Massoli, P., Nguyen, T. B., Crounse, J. D., Hu, W., Day, D. A., Tyndall, G. S., Henze, D. K., Rivera-Rios, J. C., Nowak, J. B., Kimmel, J. R., Mauldin, R. L., Stark, H., Jayne, J. T., Sipilä, M., Junninen, H., St. Clair, J. M., Zhang, X., Feiner, P. A., Zhang, L., Miller, D. O., Brune, W. H., Keutsch, F. N., Wennberg, P. O., Seinfeld, J. H., Worsnop, D. R., Jimenez, J. L. and Canagaratna, M. R.: Formation of Low Volatility Organic Compounds and Secondary Organic Aerosol from Isoprene Hydroxyhydroperoxide Low-NO Oxidation, *Environ. Sci. Technol.*, 49(17), 10330–10339, doi:10.1021/acs.est.5b02031, 2015.
- Kroll, J. H. and Seinfeld, J. H.: Chemistry of secondary organic aerosol: Formation and evolution of low-volatility organics in the atmosphere, *Atmos. Environ.*, 42(16), 3593–3624, doi:10.1016/j.atmosenv.2008.01.003, 2008.
- Kroll, J. H., Donahue, N. M., Jimenez, J. L., Kessler, S. H., Canagaratna, M. R., Wilson, K. R., Altieri, K. E., Mazzoleni, L. R., Wozniak, A. S., Bluhm, H., Mysak, E. R., Smith, J. D., Kolb, C. E. and Worsnop, D. R.: Carbon oxidation state as a metric for describing the chemistry of atmospheric organic aerosol, *Nat. Chem.*, 3(2), 133–139, doi:10.1038/nchem.948, 2011.
- Kwok, E. S. C. and Atkinson, R.: Estimation of hydroxyl radical reaction rate constants for gas-phase organic compounds using a structure-reactivity relationship: An update, *Atmos. Environ.*, 29(14), 1685–1695, doi:10.1016/1352-2310(95)00069-B, 1995.
- Lambe, A., Massoli, P., Zhang, X., Canagaratna, M., Nowak, J., Daube, C., Yan, C., Nie, W., Onasch, T., Jayne, J.,

- Kolb, C., Davidovits, P., Worsnop, D. and Brune, W.: Controlled nitric oxide production via $O(1D) + N_2O$ reactions for use in oxidation flow reactor studies, *Atmos. Meas. Tech.*, 10(6), 2283–2298, doi:10.5194/amt-10-2283-2017, 2017.
- Lambe, A. T., Krechmer, J. E., Peng, Z., Casar, J. R., Carrasquillo, A. J., Raff, J. D., Jimenez, J. L. and Worsnop, D. R.: HO_x and NO_x production in oxidation flow reactors via photolysis of isopropyl nitrite, isopropyl nitrite-d 7, and 1,3-propyl dinitrite at $\lambda = 254, 350$, and 369 nm, *Atmos. Meas. Tech.*, 12(1), 299–311, doi:10.5194/amt-12-299-2019, 2019.
- Lee, B. H., Lopez-Hilfiker, F. D., Mohr, C., Kurtén, T., Worsnop, D. R. and Thornton, J. A.: An iodide-adduct high-resolution time-of-flight chemical-ionization mass spectrometer: Application to atmospheric inorganic and organic compounds, *Environ. Sci. Technol.*, 48(11), 6309–6317, doi:10.1021/es500362a, 2014.
- Li, H., Riva, M., Rantala, P., Heikkinen, L., Daellenbach, K., Krechmer, J. E., Flaud, P.-M., Worsnop, D., Kulmala, M., Villenave, E., Perraudin, E., Ehn, M. and Bianchi, F.: Terpenes and their oxidation products in the French Landes forest: insight from Vocus PTR-TOF measurements, *Atmos. Chem. Phys. Discuss.*, (September), 1–29, doi:10.5194/acp-2019-741, 2019.
- Li, R., Palm, B. B., Ortega, A. M., Hlywiak, J., Hu, W., Peng, Z., Day, D. A., Knote, C., Brune, W. H., De Gouw, J. A. and Jimenez, J. L.: Modeling the radical chemistry in an oxidation flow reactor: Radical formation and recycling, sensitivities, and the OH exposure estimation equation, *J. Phys. Chem. A*, 119(19), 4418–4432, doi:10.1021/jp509534k, 2015.
- Li, Y. and Wang, L.: The atmospheric oxidation mechanism of 1,2,4-trimethylbenzene initiated by OH radicals, *Phys. Chem. Chem. Phys.*, 16(33), 17908, doi:10.1039/C4CP02027H, 2014.
- Lopez-Hilfiker, F. D., Mohr, C., Ehn, M., Rubach, F., Kleist, E., Wildt, J., Mentel, T. F., Lutz, A., Hallquist, M., Worsnop, D. and Thornton, J. A.: A novel method for online analysis of gas and particle composition: Description and evaluation of a filter inlet for gases and AEROSols (FIGAERO), *Atmos. Meas. Tech.*, 7, 983–1001, doi:10.5194/amt-7-983-2014, 2014.
- Lopez-Hilfiker, F. D., Iyer, S., Mohr, C., Lee, B. H., D’ambro, E. L., Kurtén, T. and Thornton, J. A.: Constraining the sensitivity of iodide adduct chemical ionization mass spectrometry to multifunctional organic molecules using the collision limit and thermodynamic stability of iodide ion adducts, *Atmos. Meas. Tech.*, 9(4), 1505–1512, doi:10.5194/amt-9-1505-2016, 2016.
- Mentel, T. F., Springer, M., Ehn, M., Kleist, E., Pullinen, I., Kurtén, T., Rissanen, M., Wahner, A. and Wildt, J.: Formation of highly oxidized multifunctional compounds: Autoxidation of peroxy radicals formed in the ozonolysis of alkenes - Deduced from structure-product relationships, *Atmos. Chem. Phys.*, 15(12), 6745–6765, doi:10.5194/acp-15-6745-2015, 2015.
- Molteni, U., Bianchi, F., Klein, F., Haddad, I. El, Frege, C., Rossi, M. J., Dommen, J. and Baltensperger, U.: Formation of highly oxygenated organic molecules from aromatic compounds, *Atmos. Chem. Phys.*, 18, 1909–1921, doi:10.5194/acp-18-1909-2018, 2018a.
- Molteni, U., Bianchi, F., Klein, F., El Haddad, I., Frege, C., Rossi, M. J., Dommen, J. and Baltensperger, U.: Formation of highly oxygenated organic molecules from aromatic compounds, *Atmos. Chem. Phys.*, 18(3), 1909–1921, doi:10.5194/acp-18-1909-2018, 2018b.
- Nah, T., Sanchez, J., Boyd, C. M. and Ng, N. L.: Photochemical Aging of α -pinene and β -pinene Secondary Organic Aerosol formed from Nitrate Radical Oxidation, *Environ. Sci. Technol.*, 50(1), 222–231, doi:10.1021/acs.est.5b04594, 2016.
- Ng, N. L., Canagaratna, M. R., Zhang, Q., Jimenez, J. L., Tian, J., Ulbrich, I. M., Kroll, J. H., Docherty, K. S., Chhabra, P. S., Bahreini, R., Murphy, S. M., Seinfeld, J. H., Hildebrandt, L., Donahue, N. M., Decarlo, P. F., Lanz, V. A., Prévôt, A. S. H., Dinar, E., Rudich, Y. and Worsnop, D. R.: Organic aerosol components observed in Northern Hemispheric datasets from Aerosol Mass Spectrometry, *Atmos. Chem. Phys.*, 10(10), 4625–4641, doi:10.5194/acp-10-4625-2010, 2010.
- Orlando, J. J. and Tyndall, G. S.: Laboratory studies of organic peroxy radical chemistry: An overview with emphasis on recent issues of atmospheric significance, *Chem. Soc. Rev.*, 41(19), 6294–6317, doi:10.1039/c2cs35166h, 2012.
- Otkjær, R. V., Jakobsen, H. H., Tram, C. M. and Kjaergaard, H. G.: Calculated Hydrogen Shift Rate Constants in Substituted Alkyl Peroxy Radicals, *J. Phys. Chem. A*, 122(43), 8665–8673, doi:10.1021/acs.jpca.8b06223, 2018.
- Peng, Z., Day, D. A., Stark, H., Li, R., Lee-Taylor, J., Palm, B. B., Brune, W. H. and Jimenez, J. L.: HO_x radical chemistry in oxidation flow reactors with low-pressure mercury lamps systematically examined by modeling, *Atmos. Meas. Tech.*, 8, 4863–4890, doi:10.5194/amt-8-4863-2015, 2015.
- Richters, S., Herrmann, H. and Berndt, T.: Different pathways of the formation of highly oxidized multifunctional

- organic compounds (HOMs) from the gas-phase ozonolysis of β -caryophyllene, *Atmos. Chem. Phys.*, 16(15), 9831–9845, doi:10.5194/acp-16-9831-2016, 2016.
- Rissanen, M. P.: NO₂ Suppression of Autoxidation-Inhibition of Gas-Phase Highly Oxidized Dimer Product Formation, *ACS Earth Sp. Chem.*, 2(11), 1211–1219, doi:10.1021/acsearthspacechem.8b00123, 2018.
- Rissanen, M. P., Kurtén, T., Sipilä, M., Thornton, J. A., Kangasluoma, J., Sarnela, N., Junninen, H., Jørgensen, S., Schallhart, S., Kajos, M. K., Taipale, R., Springer, M., Mentel, T. F., Ruuskanen, T., Petäjä, T., Worsnop, D. R., Kjaergaard, H. G. and Ehn, M.: The formation of highly oxidized multifunctional products in the ozonolysis of cyclohexene, *J. Am. Chem. Soc.*, 136(44), 15596–15606, doi:10.1021/ja507146s, 2014.
- Rissanen, M. P., Kurtén, T., Sipilä, M., Thornton, J. A., Kausiala, O., Garmash, O., Kjaergaard, H. G., Petäjä, T., Worsnop, D. R., Ehn, M. and Kulmala, M.: Effects of chemical complexity on the autoxidation mechanisms of endocyclic alkene ozonolysis products: From methylcyclohexenes toward understanding α -pinene, *J. Phys. Chem. A*, 119(19), 4633–4650, doi:10.1021/jp510966g, 2015.
- Riva, M., Rantala, P., Krechmer, J. E., Peräkylä, O., Zhang, Y., Heikkinen, L., Garmash, O., Yan, C., Kulmala, M., Worsnop, D. and Ehn, M.: Evaluating the performance of five different chemical ionization techniques for detecting gaseous oxygenated organic species, *Atmos. Meas. Tech.*, 12, 2403–2421, doi:10.5194/amt-12-2403-2019, 2019.
- Saunders, S. M., Jenkin, M. E., Derwent, R. G. and Pilling, M. J.: Protocol for the development of the Master Chemical Mechanism, MCM v3 (Part A): Tropospheric degradation of non-aromatic volatile organic compounds, *Atmos. Chem. Phys.*, 3(1), 161–180, doi:10.5194/acp-3-161-2003, 2003.
- Stolzenburg, D., Fischer, L., Vogel, A. L., Heinritzi, M., Schervish, M., Simon, M., Wagner, A. C., Dada, L., Ahonen, L. R., Amorim, A., Baccarini, A., Bauer, P. S., Baumgartner, B., Bergen, A., Bianchi, F., Breitenlechner, M., Brilke, S., Mazon, S. B., Chen, D., Dias, A., Draper, D. C., Duplissy, J., Haddad, I. El, Finkenzeller, H., Frege, C., Fuchs, C., Garmash, O., Gordon, H., He, X., Helm, J., Hofbauer, V., Hoyle, C. R., Kim, C., Kirkby, J., Kontkanen, J., Kürten, A., Lampilahti, J., Lawler, M., Lehtipalo, K., Leiminger, M., Mai, H., Mathot, S., Mentler, B., Molteni, U., Nie, W., Nieminen, T., Nowak, J. B., Ojdanic, A., Onnela, A., Passananti, M., Petäjä, T., Quéléver, L. L. J., Rissanen, M. P., Sarnela, N., Schallhart, S., Tauber, C., Tomé, A., Wagner, R., Wang, M., Weitz, L., Wimmer, D., Xiao, M., Yan, C., Ye, P., Zha, Q., Baltensperger, U., Curtius, J., Dommen, J., Flagan, R. C., Kulmala, M., Smith, J. N., Worsnop, D. R., Hansel, A., Donahue, N. M. and Winkler, P. M.: Rapid growth of organic aerosol nanoparticles over a wide tropospheric temperature range, *Proc. Natl. Acad. Sci. U. S. A.*, 115(37), 9122–9127, doi:10.1073/pnas.1807604115, 2018.
- Teng, A. P., Crounse, J. D. and Wennberg, P. O.: Isoprene Peroxy Radical Dynamics, *J. Am. Chem. Soc.*, 139(15), 5367–5377, doi:10.1021/jacs.6b12838, 2017.
- Tröstl, J., Chuang, W. K., Gordon, H., Heinritzi, M., Yan, C., Molteni, U., Ahlm, L., Frege, C., Bianchi, F., Wagner, R., Simon, M., Lehtipalo, K., Williamson, C., Craven, J. S., Duplissy, J., Adamov, A., Almeida, J., Bernhammer, A. K., Breitenlechner, M., Brilke, S., Dias, A., Ehrhart, S., Flagan, R. C., Franchin, A., Fuchs, C., Guida, R., Gysel, M., Hansel, A., Hoyle, C. R., Jokinen, T., Junninen, H., Kangasluoma, J., Keskinen, H., Kim, J., Krapf, M., Kürten, A., Laaksonen, A., Lawler, M., Leiminger, M., Mathot, S., Möhler, O., Nieminen, T., Onnela, A., Petäjä, T., Piel, F. M., Miettinen, P., Rissanen, M. P., Rondo, L., Sarnela, N., Schobesberger, S., Sengupta, K., Sipilä, M., Smith, J. N., Steiner, G., Tomé, A., Virtanen, A., Wagner, A. C., Weingartner, E., Wimmer, D., Winkler, P. M., Ye, P., Carslaw, K. S., Curtius, J., Dommen, J., Kirkby, J., Kulmala, M., Riipinen, I., Worsnop, D. R., Donahue, N. M. and Baltensperger, U.: The role of low-volatility organic compounds in initial particle growth in the atmosphere, *Nature*, 533(7604), 527–531, doi:10.1038/nature18271, 2016.
- Tsiligiannis, E., Hammes, J., Salvador, C. M., Mentel, T. F. and Hallquist, M.: Effect of NO_x on 1,3,5-trimethylbenzene (TMB) oxidation product distribution and particle formation, *Atmos. Chem. Phys.*, 19(23), 15073–15086, doi:10.5194/acp-19-15073-2019, 2019.
- Wang, S., Wu, R., Berndt, T., Ehn, M. and Wang, L.: Formation of Highly Oxidized Radicals and Multifunctional Products from the Atmospheric Oxidation of Alkylbenzenes, *Environ. Sci. Technol.*, 51(15), 8442–8449, doi:10.1021/acs.est.7b02374, 2017.
- Wang, Y., Riva, M., Xie, H. and Heikkinen, L.: Formation of highly oxygenated organic molecules from chlorine atom initiated oxidation of α -pinene, *Atmos. Chem. Phys. Discuss.*, (October), 1–31, doi:10.5194/acp-2019-807, 2019.
- Yuan, B., Koss, A. R., Warneke, C., Coggon, M., Sekimoto, K. and De Gouw, J. A.: Proton-Transfer-Reaction Mass Spectrometry: Applications in Atmospheric Sciences, *Chem. Rev.*, 117(21), 13187–13229, doi:10.1021/acs.chemrev.7b00325, 2017.
- Zaytsev, A., Koss, A. R., Breitenlechner, M., Krechmer, J. E., Nihill, K. J., Lim, C. Y., Rowe, J. C., Cox, J. L.,

- Moss, J., Roscioli, J. R., Canagaratna, M. R., Worsnop, D. R., Kroll, J. H. and Keutsch, F. N.: Mechanistic study of the formation of ring-retaining and ring-opening products from the oxidation of aromatic compounds under urban atmospheric conditions, *Atmos. Chem. Phys.*, 19(23), 15117–15129, doi:10.5194/acp-19-15117-2019, 2019.
- Zhang, Q., Jimenez, J. L., Canagaratna, M. R., Allan, J. D., Coe, H., Ulbrich, I., Alfarra, M. R., Takami, A., Middlebrook, A. M., Sun, Y. L., Dzepina, K., Dunlea, E., Docherty, K., DeCarlo, P. F., Salcedo, D., Onasch, T., Jayne, J. T., Miyoshi, T., Shimon, A., Hatakeyama, S., Takegawa, N., Kondo, Y., Schneider, J., Drewnick, F., Borrmann, S., Weimer, S., Demerjian, K., Williams, P., Bower, K., Bahreini, R., Cottrell, L., Griffin, R. J., Rautiainen, J., Sun, J. Y., Zhang, Y. M. and Worsnop, D. R.: Ubiquity and dominance of oxygenated species in organic aerosols in anthropogenically-influenced Northern Hemisphere midlatitudes, *Geophys. Res. Lett.*, 34(13), 1–6, doi:10.1029/2007GL029979, 2007.
- Zhao, Y., Thornton, J. A. and Pye, H. O. T.: Quantitative constraints on autoxidation and dimer formation from direct probing of monoterpene-derived peroxy radical chemistry, *Proc. Natl. Acad. Sci.*, 115(48), 12142–12147, doi:10.1073/pnas.1812147115, 2018.
- Ziemann, P. J. and Atkinson, R.: Kinetics, products, and mechanisms of secondary organic aerosol formation, *Chem. Soc. Rev.*, 41(19), 6582–6605, doi:10.1039/c2cs35122f, 2012.

Table 1 Summary of experimental conditions.

#	Precursor	Experimental condition	Precursor concentration (ppb)	Consumption of precursor (%)	RH (%)	Total flow rate (slpm)	O ₃ concentration (ppb)
1	1,2,4-TMB	OH	158	59.3	12.5	10	712
2	1,3,5-TMB	OH	118	62.8	13.6	10	845
3	1,2,3-TMB	OH	214	58.4	8.1	10	1426
4	1,2,4-(1-methyl-D3)-TMB	OH	155	62.0	11.6	10	1003
5	1,2,4-(2-methyl-D3)-TMB	OH	169	61.8	12.5	10	776
6	1,2,4-(4-methyl-D3)-TMB	OH	166	62.8	11.5	10	886
7	1,2,4-TMB	Low NO _x (<u>2.5 ppb NO + 89.5 ppb NO₂</u>) ^a (<u>0.8 ppb NO_x</u>)	170	61.5	12.7	10.4	944
8	1,2,4-TMB	Higher NO _x (<u>6.5 ppb NO_x</u>) (<u>2.9 ppb NO + 292.4 ppb NO₂</u>) ^a	145	69.7	9.3	10.4	3911

^a Modelled mathematically-averaged NO/NO₂ concentrations in the OFR are shown here because of the malfunction of a NO_x monitor. The model underestimates [NO] and [NO₂] by up to a factor of 2, according to separate experiments that are not presented.

Table 2. Oxidation products of 1,2,4-TMB in categories of carbonyl, hydroxyl, and hydroperoxyl according to their molecular mass, as well as the potential peroxy radicals. Numbers in the parenthesis denote the relative intensity detected by Nitrate CI-API-TOF in the OH-initiated oxidation of 1,2,4-TMB when that of the largest HOM signal ($C_9H_{16}O_8$) is arbitrarily set to be 100%. The relative intensity has been corrected with the relative transmission efficiency of Nitrate CI-API-TOF.

The potential peroxy radical <i>m</i>	Carbonyl <i>m</i> -17	Hydroxyl <i>m</i> -15	Hydroperoxyl <i>m</i> +1
$C_9H_{13}O_7^{\bullet}$	$C_9H_{12}O_6^{a,b,c,d}$ (9.2 %)	$C_9H_{14}O_6^{a,b,c,d}$ (20.3 %)	$C_9H_{14}O_7^{b,c,d}$ (50.4 %)
$C_9H_{13}O_8^{\bullet}$	$C_9H_{12}O_7^{b,c,d}$ (54.4 %)	$C_9H_{14}O_7^{b,c,d}$ (50.4 %)	$C_9H_{14}O_8^{c,d}$ (51.6 %)
$C_9H_{13}O_9^{\bullet}$	$C_9H_{12}O_8^d$ (17.3 %)	$C_9H_{14}O_8^{c,d}$ (51.6 %)	$C_9H_{14}O_9^d$ (29.1 %)
$C_9H_{13}O_{10}^{\bullet}$	$C_9H_{12}O_9^d$ (14.9 %)	$C_9H_{14}O_9^d$ (29.1 %)	$C_9H_{14}O_{10}^d$ (19.8 %)
$C_9H_{15}O_7^{\bullet}$	$C_9H_{14}O_6^{a,b,c,d}$ (20.3 %)	$C_9H_{16}O_6^{b,c,d}$ (2.3 %)	$C_9H_{16}O_7^{b,c,d}$ (23.5 %)
$C_9H_{15}O_8^{\bullet}$	$C_9H_{14}O_7^{b,c,d}$ (50.4 %)	$C_9H_{16}O_7^{b,c,d}$ (23.5 %)	$C_9H_{16}O_8^{c,d}$ (100 %)
$C_9H_{15}O_9^{\bullet}$	$C_9H_{14}O_8^{c,d}$ (51.6 %)	$C_9H_{16}O_8^{c,d}$ (100 %)	$C_9H_{16}O_9^d$ (40.5 %)
$C_9H_{15}O_{10}^{\bullet}$	$C_9H_{14}O_9^d$ (29.1 %)	$C_9H_{16}O_9^d$ (40.5 %)	$C_9H_{16}O_{10}^d$ (7.1 %)

^a These compounds are listed in the MCM mechanism of 1,2,4-TMB where they are formed by multiple OH oxidation steps.

^b These compounds were detected by Vocus PTR.

^c These compounds were detected by Iodide CI-TOF in both gas and particle phase.

^d These compounds were detected by Nitrate CI-API-TOF.

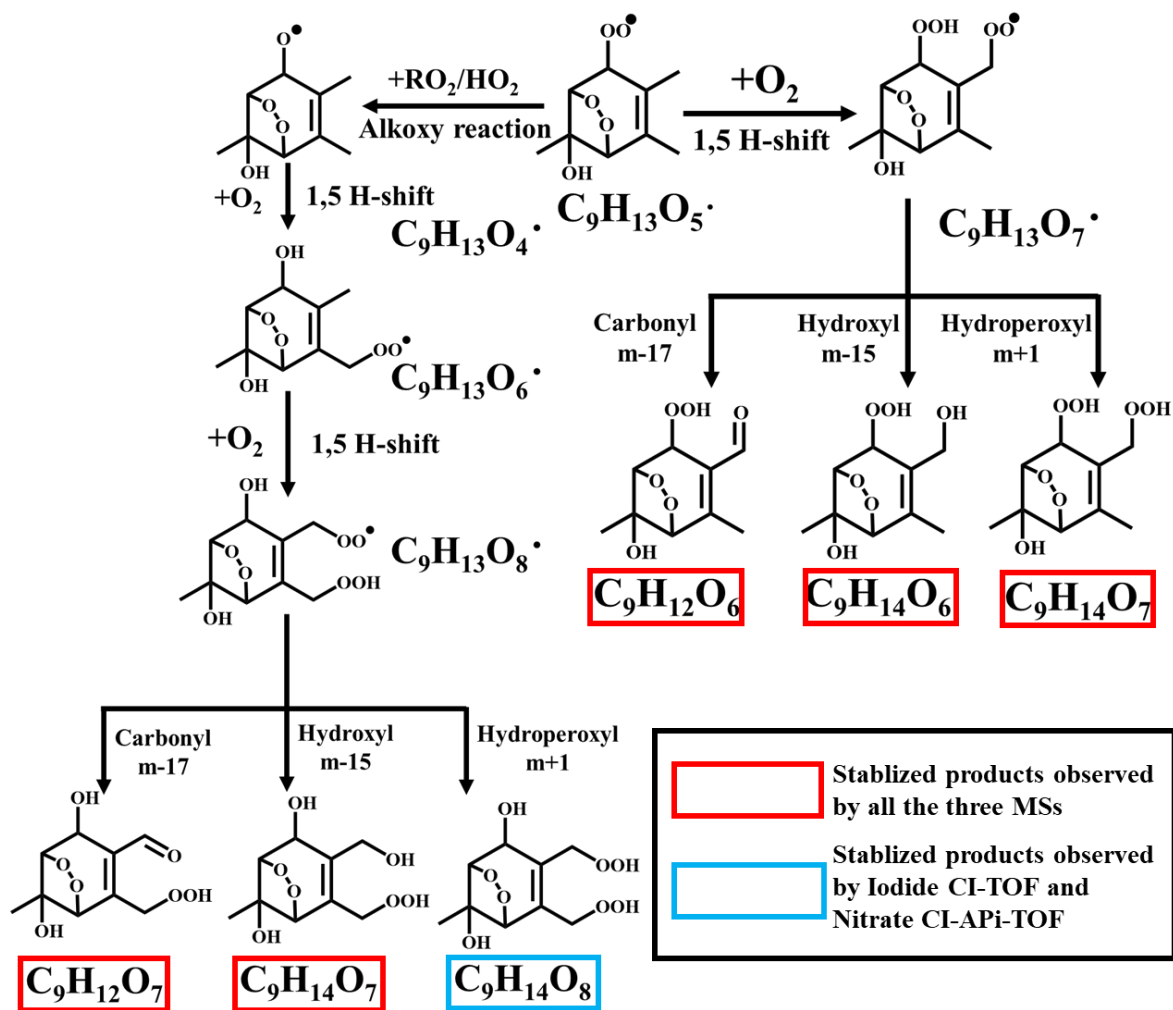
Table 3. Partially deuterated C9 products observed by Vocus PTR and/or Nitrate CI-APi-TOF. “V” and “N” denote observation by Vocus PTR and Nitrate CI-APi-TOF, respectively, whereas “-” means that the product was not observed by any instrument.

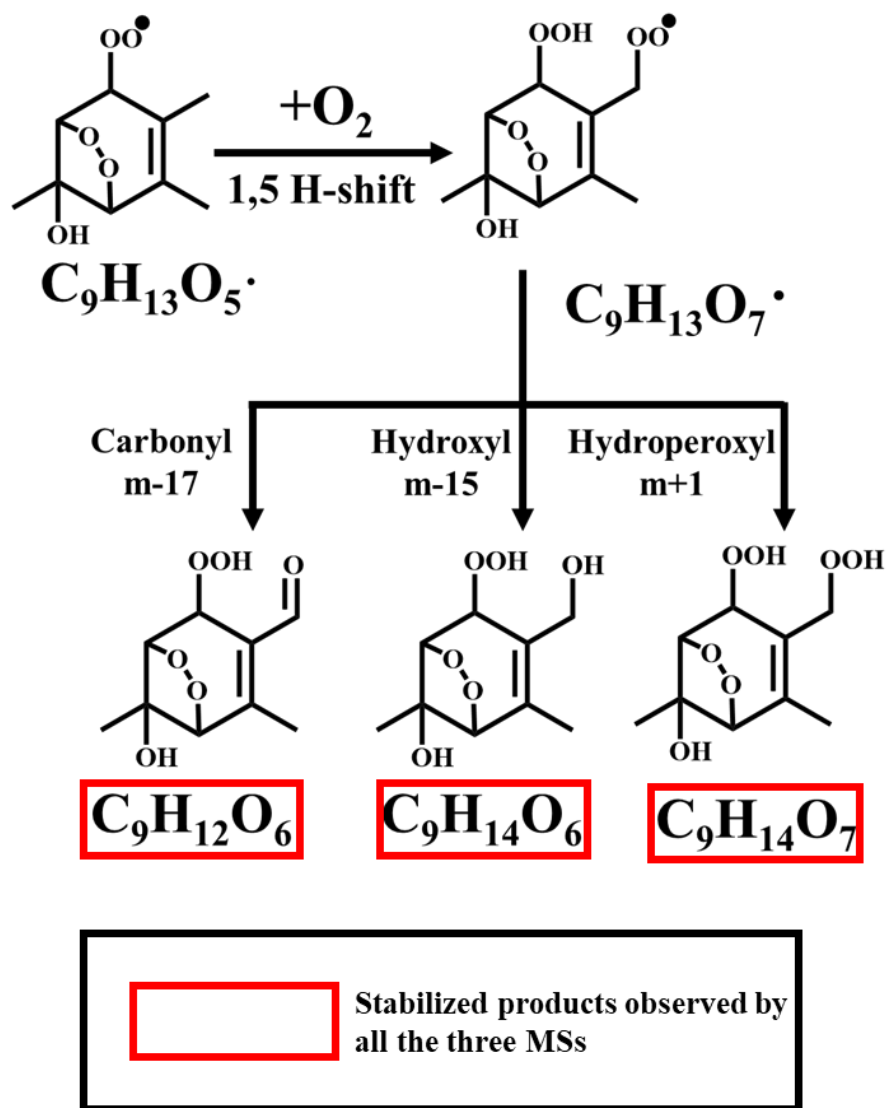
	1,2,4-(1-methyl-D3)- TMB	1,2,4-(2-methyl-D3)- TMB	1,2,4-(4-methyl-D3)- TMB
$C_9H_{10}D_2O_6$	V, N	-	-
$C_9H_{10}D_2O_7$	V	-	-
$C_9H_{12}D_2O_8$	-	-	N

Scheme Captions

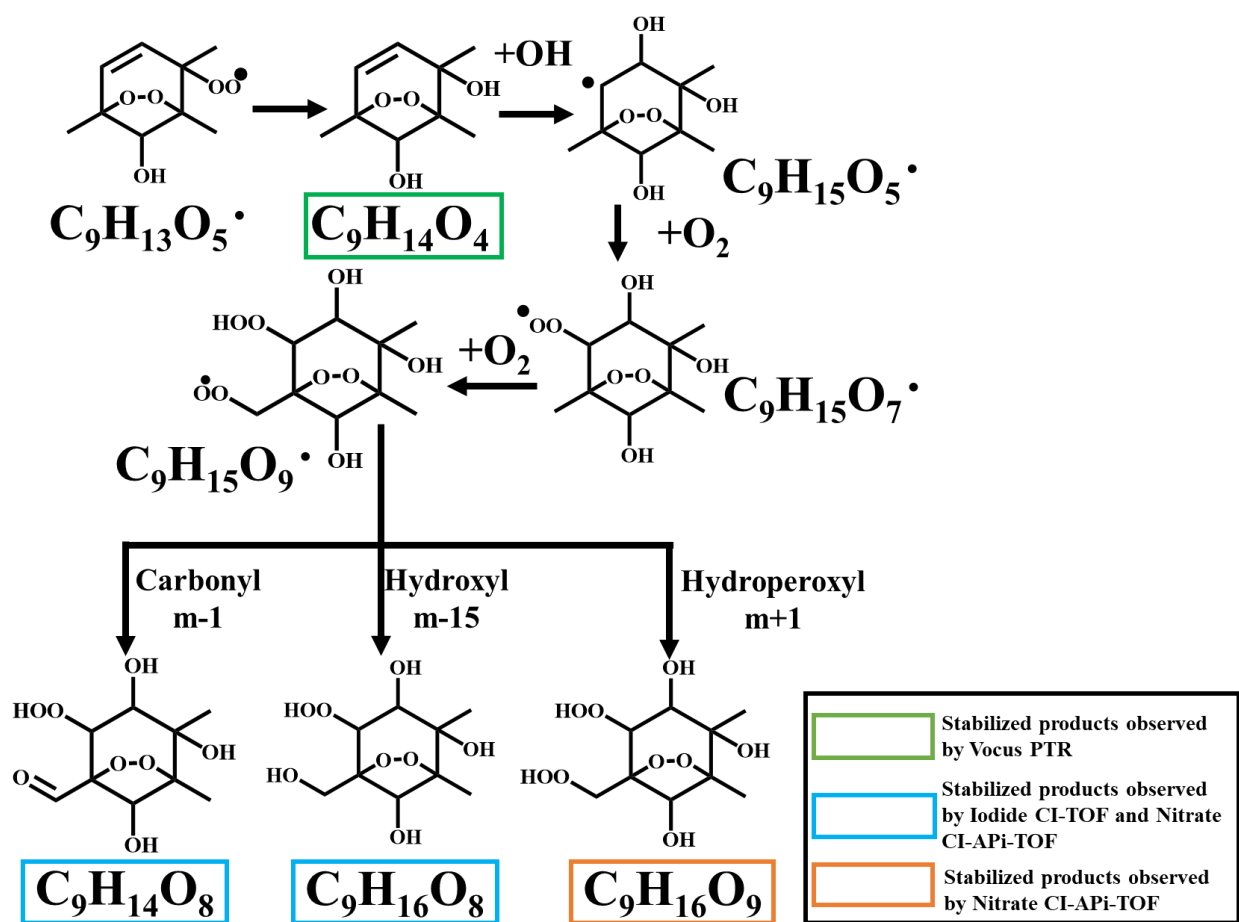
Scheme 1. A proposed autoxidation reaction scheme involving a bicyclic peroxy radical of $C_9H_{13}O_5\cdot$.

Scheme 2. A proposed autoxidation reaction scheme involving a bicyclic peroxy radical of $C_9H_{13}O_5\cdot$. Note that the reaction has been terminated with the formation of $C_9H_{14}O_4$ and re-initiated by a second OH attack.





Scheme 1



Scheme 2

Figure Captions

Figure 1. Schematics of experimental setup.

Figure 2. Comparison of C7-C9 products observed in the OH-initiated oxidation of 1,2,4-TMB (Exp. #1 in Table 1) with those listed in the MCM mechanism (Bloss et al., 2005). Filled red, orange, and green circles denote observation by Nitrate CI-APi-TOF, Iodide CI-TOF, and Vocus PTR, respectively, whereas open blue circles represent MCM species. The radius of filled circles are proportional to the signals of the compounds in each instrument. The signal of the most abundant product for each instrument is arbitrarily set to be 100%, but note that the arbitrary signals are not comparable among instruments. Symbols have been offset horizontally to avoid overlap.

Figure 3. Distribution of C9 products formed from OH-initiated reactions of TMBs (Exp. #1- 3 in Table 1) by (a) Vocus PTR, (b) Iodide CI-TOF for the gas phase, (c) Iodide CI-TOF for particle phase, and (d) Nitrate CI-APi-TOF. The yield of the most abundant product for each instrument is arbitrarily set to be 100%, but note that the arbitrary yields are not comparable among instruments. Also note that signal of Vocus PTR was processed in a logarithmic way before calculating the arbitrary yield.

Figure 4. (a) Distribution of $C_{18}H_{24}O_{8-13}$ and $C_{18}H_{26}O_{8-15}$ products formed from TMB oxidation experiments (Exp. #1-3 in Table 1), as measured by Nitrate CI-APi-TOF; (b) Distribution of $C_{18}H_{28}O_{9-15}$ and $C_{18}H_{30}O_{12-15}$ formed from TMB oxidation experiments (Exp. #1-3 in Table 1), as measure by Nitrate CI-APi-TOF; and (c) The total signal of C18 products formed from TMB oxidation experiments (Exp. #1-3 in Table 1), as measure by Nitrate CI-APi-TOF.

Figure 5. Relative contribution of C9 and C18 products formed from TMB oxidation experiments, as measured by Nitrate CI-APi-TOF. The relative intensity has been corrected with the relative transmission efficiency.

Figure 6. Comparison of C9 products detected by Nitrate CI-APi-TOF with zero, one or two nitrogen atoms formed from 1,2,4-TMB oxidation with different NO_x settings.

Figure 7. (a) Comparison of C18 HOMs formed from 1,2,4-TMB oxidation with different NO_x settings; and (b) Distribution of C18 organonitrates fomed from 1,2,4-TMB oxidation.

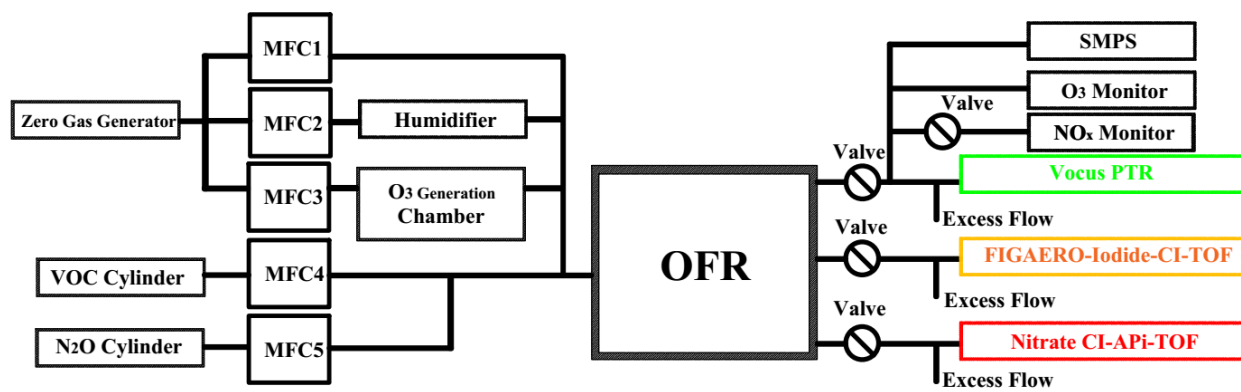


Figure 1

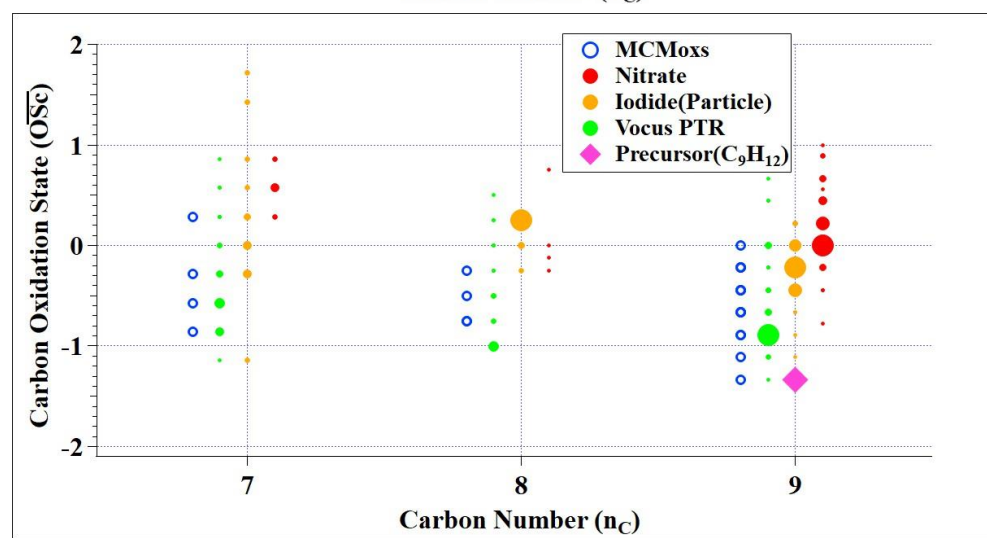
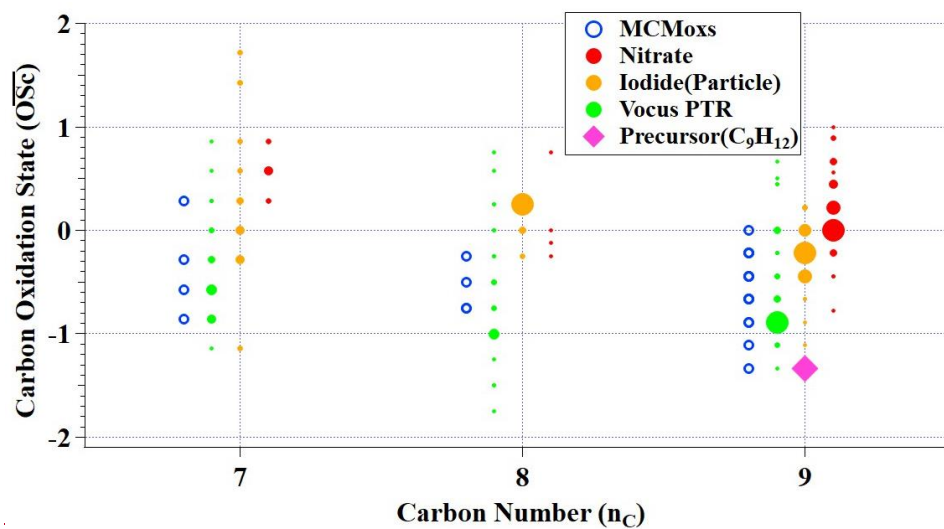


Figure 2

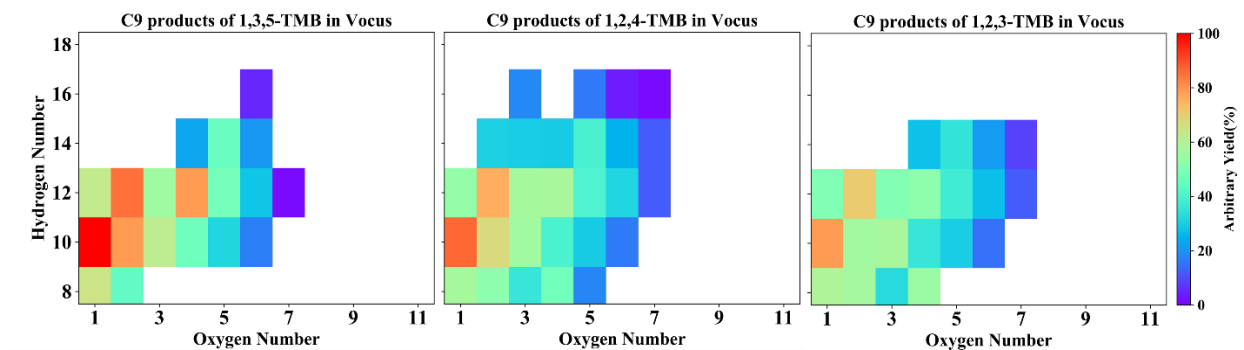


Figure 3a

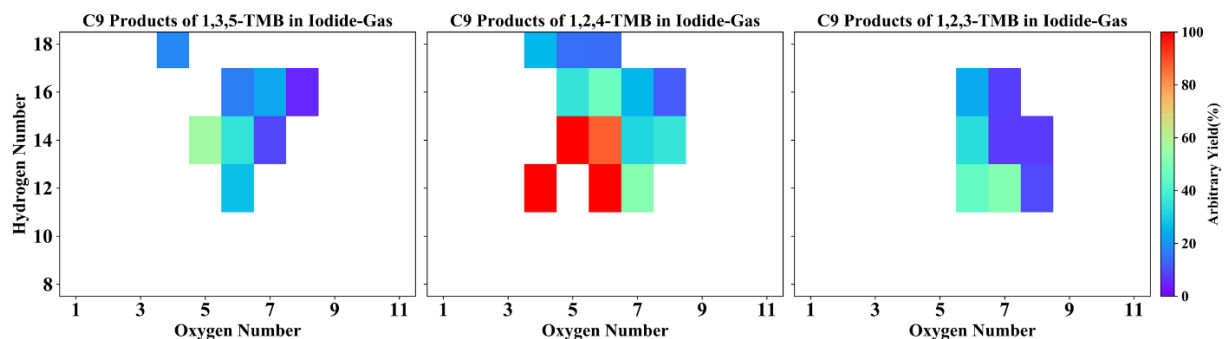


Figure 3b

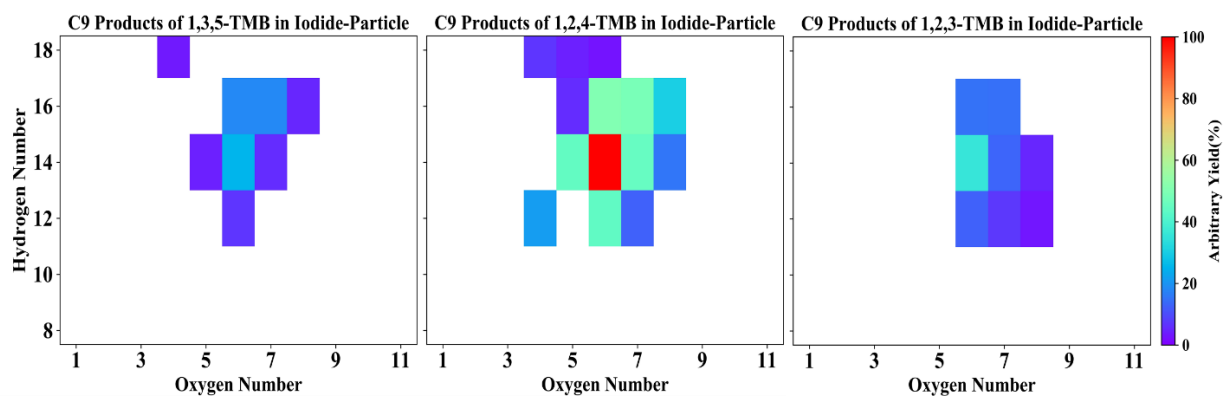


Figure 3c

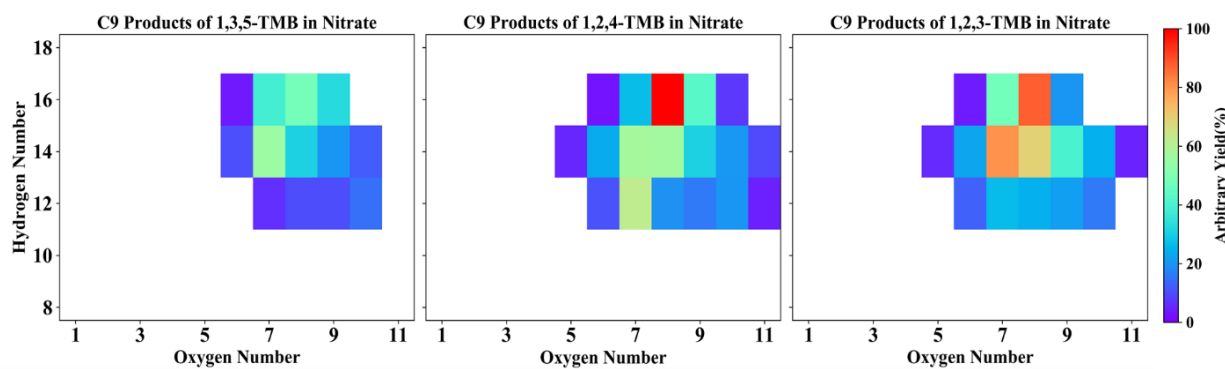


Figure 3d

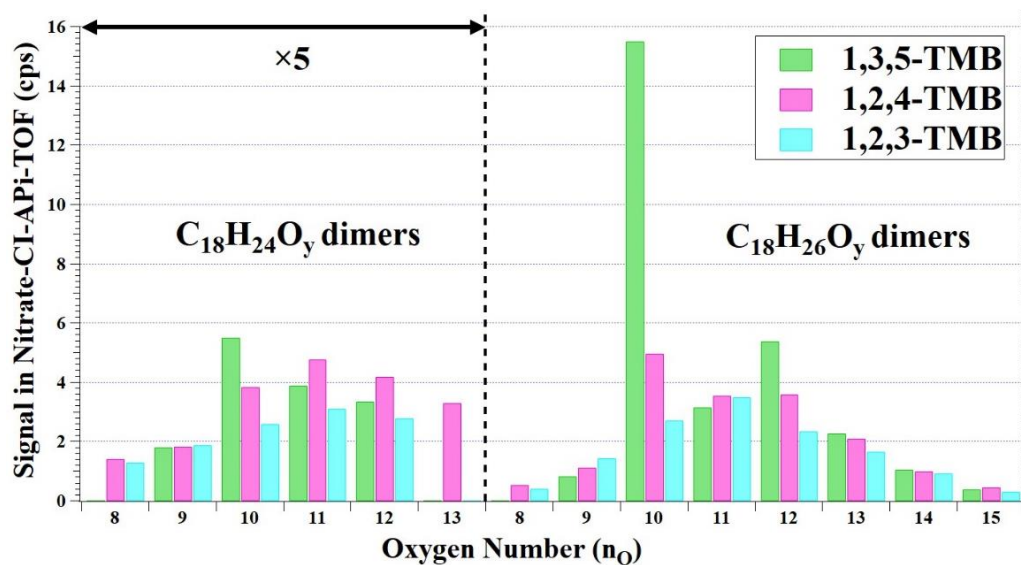


Figure 4a

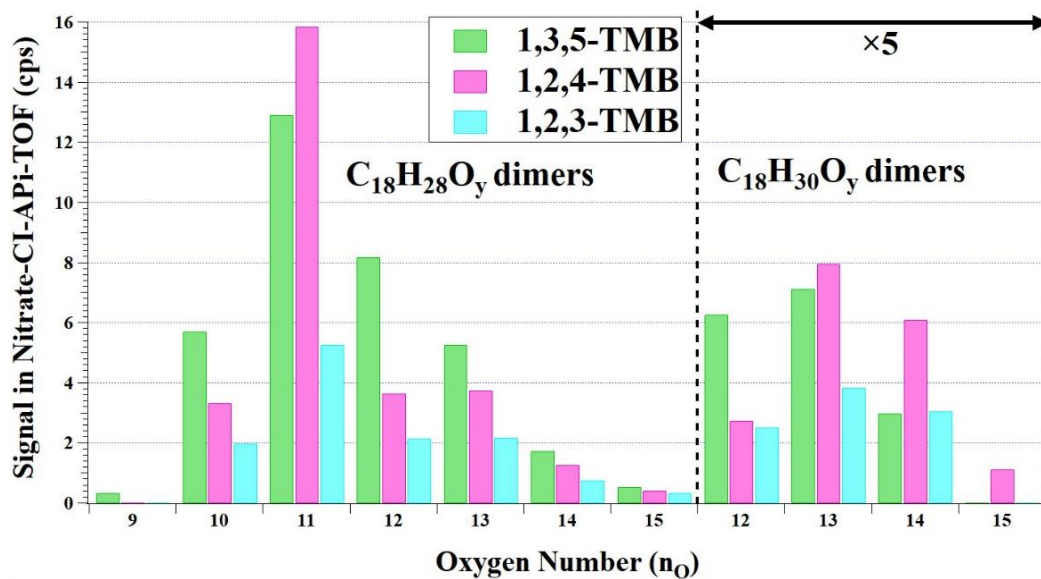


Figure 4b

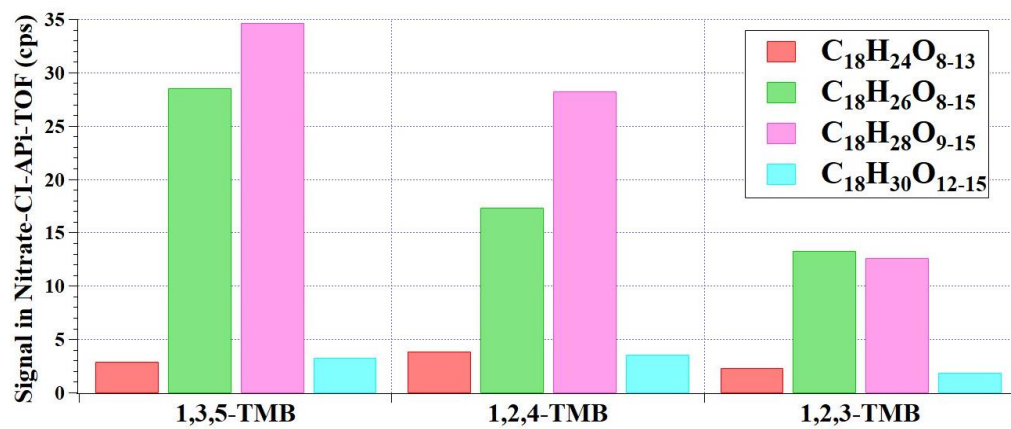


Figure 4c

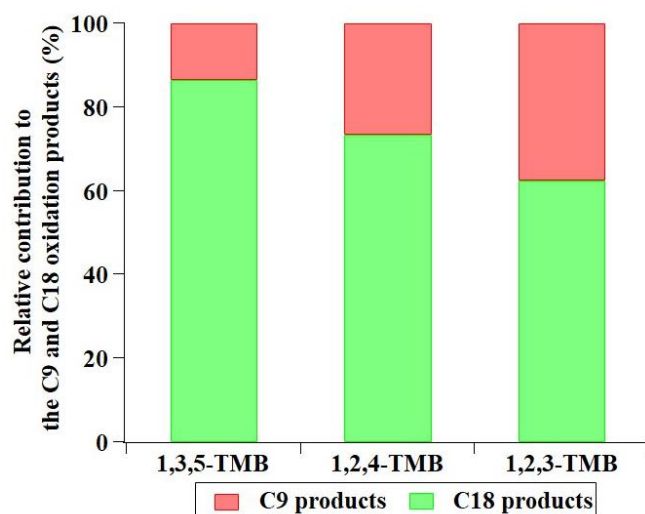


Figure 5

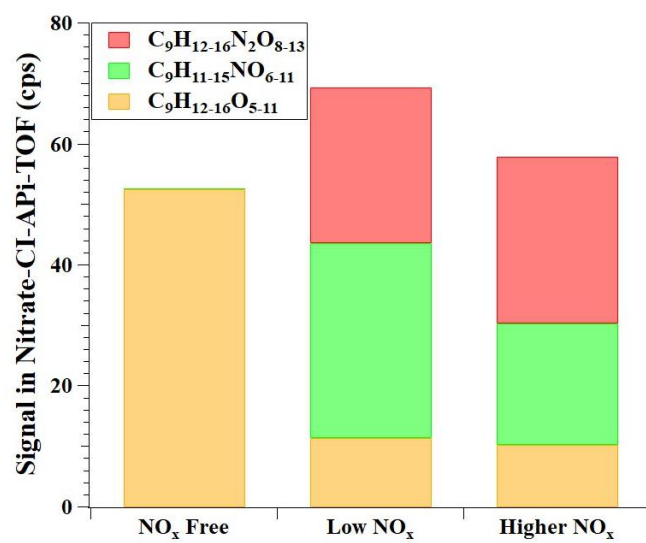


Figure 6

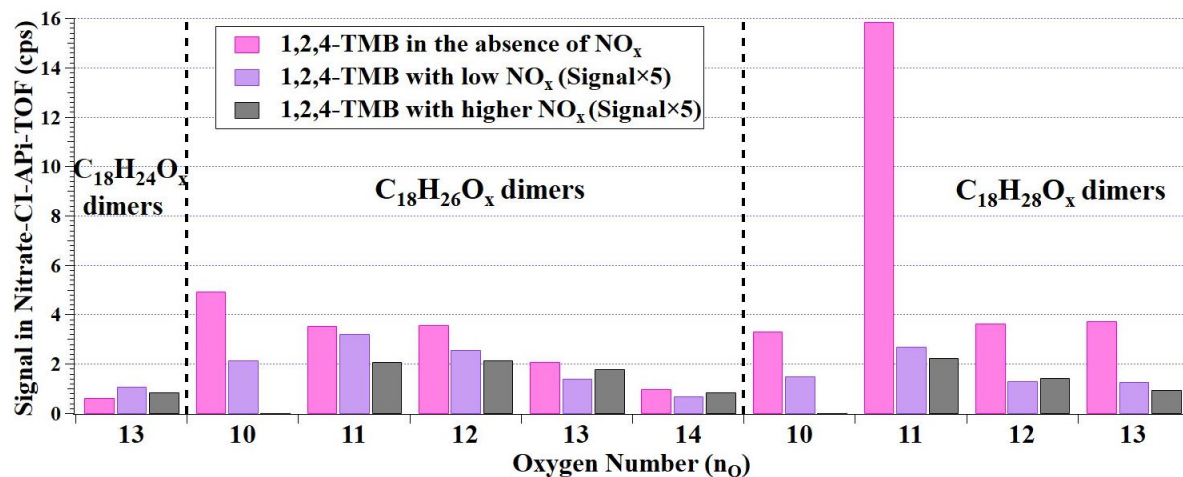


Figure 7a

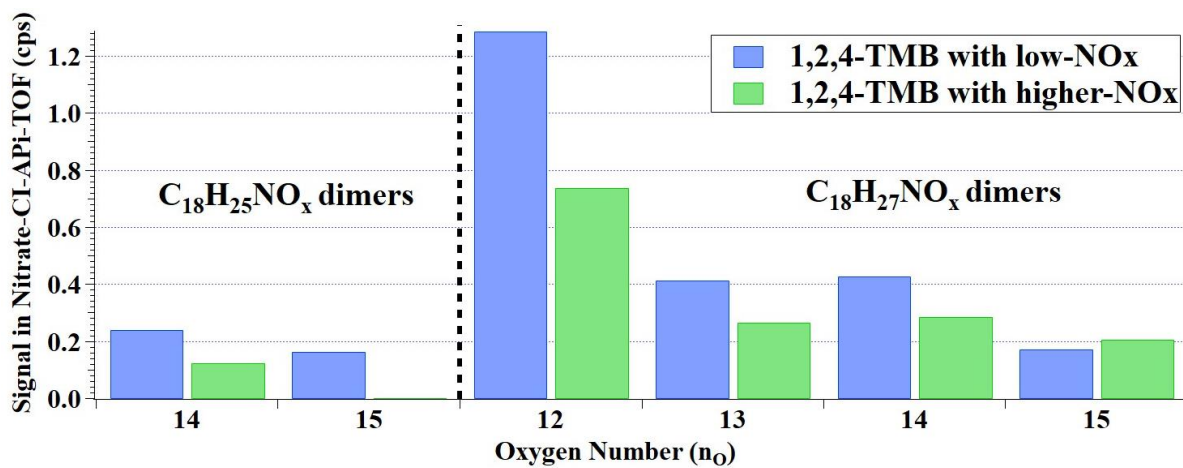


Figure 7b